Comparison of JET AVDE disruption data with M3D simulations and implications for ITER

Comparison of JET AVDE disruption data with M3D simulations and implications for ITER

H. Strauss,[1, a)] E. Joffrin,[2] V. Riccardo,[3] J. Breslau,[3] R. Paccagnella,[4] and JET Contributors[b)]

[1)] *HRS Fusion, West Orange NJ 07052 USA*

[2)] *CEA, IRFM, F-13108 Saint-Paul-lez-Durance, France*

[3)] *Princeton Plasma Physics Laboratory, Princeton NJ 08570 USA*

[4)] *Consorzio RFX and Istituto Gas Ionizzati del C.N.R., 35127 Padua, Italy*

Nonlinear 3D MHD asymmetric vertical displacement disruptions simulations have been performed using JET equilibrium reconstruction initial data. Several experimentally measured quantities are compared with the simulation. These include vertical displacement, halo current, toroidal current asymmetry, and toroidal rotation. The experimental data and the simulations are in reasonable agreement. Also compared was the correlation of the toroidal current asymmetry and the vertical displacement asymmetry. The Noll relation between asymmetric wall force and vertical current moment is verified in the simulations. Also verified is toroidal flux asymmetry. Although in many ways JET is a good predictor of ITER disruption behavior, JET and ITER can be in different parameter regimes, and extrapolating from JET data can overestimate the ITER wall force.

PACS numbers: 52.55Fa, 52.55Tn, 52.65Kj

[a)] Electronic mail: hank@hrsfusion.com

[b)] See the author list of Overview of the JET results in support to ITER by X. Litaudon et al. to be published in Nuclear Fusion Special issue: overview and summary reports from the 26th Fusion Energy Conference (Kyoto, Japan, 17-22 October 2016)

I. INTRODUCTION

A main source of predictions about ITER[1] disruptions is JET experimental data[2]. Further predictions have been made using MHD simulations[3–7]. Numerous other studies have been carried out, for example[8–14]. It is important to verify that the simulations are in agreement with JET data. This paper compares experimental data to MHD asymmetric vertical displacement event (AVDE) disruption simulations using the M3D[15] code.

It will also be pointed out in what sense JET is not a good predictor of ITER. JET and ITER can be in different parameter regimes. Although dimensional analysis indicates ITER asymmetric wall force could be 25 times larger than in JET[2], the simulations presented in this paper show a novel result, that the ITER wall force might not be much larger than in JET.

The M3D simulations were initialized with EFIT equilibrium reconstruction of JET disruption shot 71985 at $t = 67.3128s$, with magnetic field $B = 2T$[16,17], with carbon wall.

Detailed comparison of JET data with 3D MHD simulations has not been done previously. Several variables were compared in simulation and experiment and are in reasonable agreement. These include the time history of vertical position and current, halo current, asymmetric wall force, and toroidal rotation. Also compared was the correlation of the toroidal current asymmetry and the vertical displacement asymmetry, and a new analysis was provided. Toroidal flux asymmetry[16] was verified in the simulations. It is verified that the Noll relation[18,19] between asymmetric wall force and vertical current moment holds in the simulations. The comparison of JET data with 3D MHD simulation provides a validation of the M3D code.

The results obtained for the selected shot can be expected to be generally relevant to JET. The values of the compared quantities in this shot are typical of JET disruption data[2].

The simulation parameters were Lundquist number $S = 10^6$, and the resistive wall Lundquist number was $S_{wall} = \tau_{wall}/\tau_A = 250 - 1000$, where $\tau_{wall} = \mu_0 a\delta/\eta_{wall}$ is the wall magnetic field penetration time (a being the minor plasma radius, δ the wall thickness, and η_{wall} the wall resistivity), and where $\tau_A = R/v_A$ is the Alfvén time, with v_A the Alfvén speed and R the major radius. The simulation uses time units of τ_A.

An important feature of the simulations is that most of the measured quantities are independent of simulational value of S_{wall}, for a given experimental wall time. This allows simulations to be run for much shorter times than when the experimental S_{wall} is used.

In the experiment, prior to the thermal quench (TQ), $S = 10^9$, but after the TQ, $S \approx 10^5$. The wall Lundquist number is $S_{wall} = 7 \times 10^3$.

The present simulations, both the TQ and the current quench (CQ) were included.

Section II describes the simulations and experimental data, Section III deals with comparison of halo current data, Section IV describes toroidal current and toroidal flux variation, Section V is concerned with the correlation of the toroidal variation of the toroidal current and the vertical displacement. Section VI discusses the Noll relation, Section VII describes toroidal rotation, Section VIII explains the asymmetric force to be expected in ITER, and finally Section IX summarizes the results.

II. JET AVDE DISRUPTION SIMULATIONS AND EXPERIMENTAL MEASUREMENTS

The time history of the experimental data and simulation of shot 71985 are shown in Fig.1. The experimental toroidal current is denoted I_p, in MA and the vertical displacement as z_p. Time is in units of resistive wall time τ_{wall}, which in the experiment is $\tau_{wall}^{JET} = 0.005s$[20,21]. The simulated current I was driven according to the experimental current I_p in time normalized to the resistive wall time, with

$$I(t/\tau_{wall}) \propto I_p(t/\tau_{wall}^{JET}), \tag{1}$$

using the experimental time history data $I_p(t)$ for shot 71985. Here τ_{wall} is the resistive wall time in the simulation, which is less than the experimental resistive wall time. This rescaling was necessary because of computation time limitations on the simulations. As will be shown, the results are not strongly dependent on the choice of simulational τ_{wall}. An artificial electric field current controller was applied to sustain the current, which keeps the simulation current approximately equal to the experimental current. Shown in Fig.1 are simulation total current I and vertical displacement ξ, and the experimental measurements of I_p and z_p, where I , I_p are in MA and z_p, ξ are in m. The experimental data is presented in units of experimental wall time, and the simulation is in units of simulation wall time. It is noteworthy that the simulated vertical displacement ξ agrees well with z_p during the growth and initial saturation phases. This agreement holds for all values of S_{wall} that were simulated.

The initial equilibrium obtained from the equilibrium reconstruction has $q_0 < 1$, which was unstable to a helical MHD instability with poloidal and toroidal mode numbers $(m, n) = (1, 1)$ mode. This mode and the $(1, 0)$ vertical instability combine to produce the TQ by $t = 1.5\tau_{wall}$.

Fig.2 shows contour plots in a simulation with $S_{wall} = 1000$, at time $t = 3.93\tau_{wall}$ when the VDE has saturated, in the (R, Z) plane with $\phi = 0$. Fig.2(a) shows contours of poloidal magnetic flux ψ. Fig.2(b) shows the toroidal current density RJ_ϕ, with a large $(m, n) = (1, 1)$ internal kink perturbation. Fig.2(c) shows the toroidal magnetic field multiplied by R, RB_ϕ.

III. HALO CURRENT

Fig.2(d) shows the toroidal field perturbation multiplied by R, $R\delta B_\phi$, on the wall, at the same time as in Fig.2(a),(b),(c). The vertical coordinate is the toroidal angle $\phi/(2\pi)$, and the horizontal coordinate is a poloidal angle $\theta/2\pi$. The magnetic perturbation is largest along the line of the observation angle $\theta_o \approx 2\pi/3$, at the top of the JET wall, near the typical VDE strike point. Here

$$\delta B_\phi = B_\phi(\theta_o, t) - B_\phi(\theta_o, 0) \tag{2}$$

the difference between the flux at the observation angle θ_0 at times $t = 3.93\tau_{wall}$ and $t = 0$.

Halo current is the current which flows on open field lines. In JET toroidal field measurements serve as a proxy for halo current[17]

$$I_{halo}^{JET} = 2\pi R\delta B_\phi \tag{3}$$

where δB_ϕ is defined in (2).

Fig.2(d) has the largest flux perturbations at the observation angle. The JET halo current detectors measure toroidal magnetic field perturbations δB_ϕ at θ_o and at toroidal measurement angles $\phi \approx (k-1)\pi/2$, with $k = 1, \ldots 4$. The JET torus is divided into octants, in which toroidal field pick-up coils and Rogowskii coils are installed[2,17]. The halo current measurements are made in octants $1, 3, 5, 7$.

In the following several quantities will be compared in simulation and experiment. Consider the variable $f = f_0 + f_s \sin\phi + f_c \cos\phi$. Listed are definitions of the average of f and the amplitude of the toroidally varying part of f,

$$
\begin{aligned}
f &= \overline{f} + \tilde{f} \\
\tilde{f} &= f - \overline{f} = f_s \sin\phi + f_c \cos\phi \\
f_c &= \frac{1}{2}(f_5 - f_1) \\
f_s &= \frac{1}{2}(f_7 - f_3) \\
\overline{f} &= \oint f \frac{d\phi}{2\pi} = f_0 = \frac{1}{4}\left(f_1 + f_3 + f_5 + f_7\right) \\
\Delta f &= \left(\oint \tilde{f}^2 \frac{d\phi}{\pi}\right)^{1/2} = \left(f_s^2 + f_c^2\right)^{1/2} = \frac{1}{2}\left[(f_5 - f_1)^2 + (f_7 - f_3)^2\right]^{1/2}
\end{aligned}
\tag{4}
$$

Equivalent definitions are given for the case when f is represented as a Fourier series with $n = 0$ and $n = 1$ components, as in the simulations, or as a discrete set of values on four octants of a torus, as in the experiment.

Here $\overline{\delta B}$ is the average of δB_ϕ over the toroidal angles, and $\Delta(\delta B)$ is the amplitude of the toroidally varying part. The simulated values were calculated by taking Fourier components of $\delta B_\phi(\phi)$. In Fig.3 these values are plotted as halo current fractions

$$
\begin{aligned}
HF_a &= 2\pi R \frac{\overline{\delta B}_a}{I_o} \\
\Delta HF_a &= 2\pi R \frac{\Delta(\delta B)_a}{I_o}
\end{aligned}
\tag{5}
$$

for the experimental (a = exp) and simulated values (a = sim) in units of experimental and simulational wall time respectively. Here I_o is the toroidal current at time $t = 0$. In the simulation, $S_{wall} = 1000$. The magnitudes of the peak values are in reasonable agreement.

The simulations were done for several values of S_{wall}. Fig.3(b) shows the peak value in time of HF and ΔHF. The simulated values appear to converge to the experimental values, which implies that the peak values of the simulated quantities do not depend on the wall time. This allows the results to be extrapolated to the experimental value of $S_{wall} = 7 \times 10^3$. At present, computational restrictions limit the simulations to smaller values of S_{wall}.

IV. TOROIDAL CURRENT AND TOROIDAL FLUX VARIATION

Toroidal $n = 1$ variation of toroidal current was observed in JET[2,16]. The time history plot Fig.4 shows the magnitude of the toroidal current variation comparing JET and simulation.

The toroidal current asymmetry is ΔI, as defined above in (4), where the current is

$$I = \int J_\phi d^2x. \tag{6}$$

The asymmetric toroidal current can be obtained from $\nabla \cdot \mathbf{J} = 0$, or in integral form,

$$\frac{\partial I}{\partial \phi} = -\oint R J_n dl = -I_{halo}^{3D} \tag{7}$$

where the poloidal current normal to the wall is

$$J_n = \frac{1}{R}\frac{\partial (RB_\phi)}{\partial l} - \frac{1}{R}\frac{\partial B_l}{\partial \phi} \tag{8}$$

and where dl is the length element, and B_l is the component of magnetic field tangent to the wall. The 3D halo current I_{halo}^{3D} in (7) gives the net inflow or outflow of normal current at a particular toroidal angle[4] and vanishes if the current is toroidally symmetric.

In Fig.4, the experimental dimensionless current is labelled $\Delta I_p/I_p$, and the simulated value is $\Delta I/I$. The same discrete expression was used for experimental and simulated values. The agreement of the peak values is acceptable. The amplitude of $\Delta I/I$ decays more rapidly in time than the experimental data, when the total current is decaying. The current variation ΔI depends on the amplitude of the kink mode, as shown in (18),(20). This suggests that the decrease of ΔI is caused by stabilization of the kink. In turn this may be caused by decay of the total current I, which can raise the value of q. The different behavior if the simulation and the experiment may be due to the different values of S, which governs the rate of resistive decay. The fluctuations in the simulated $\Delta I/I$ may be related to fluctuations in I_p and ξ, z_p in Fig.1.

Also shown in Fig.4 is the toroidally varying toroidal magnetic flux $\Delta\Phi/\Phi$, where Φ is

$$\Phi = \int B_\phi d^2x, \tag{9}$$

and $\Delta\Phi$ is obtained using (4).

The toroidal variation of toroidal flux[16] follows from $\nabla \cdot \mathbf{B} = 0$,

$$\frac{\partial \Phi}{\partial \phi} = - \oint R B_n dl. \tag{10}$$

To estimate the ratio of current perturbations to flux perturbations in Fig.4, take $J_n \approx -\partial B_\theta/(R\partial\phi)$. Assuming an $(m,n) = (1,1)$ mode, then $J_n \approx -\partial B_\theta/(r\partial\theta)$. From approximate incompressibility (12) with large aspect ratio[15], $J_n \approx \partial B_r/\partial r \approx B_n/a$. Then (7),(10) give $\Delta I \approx \Delta\Phi/a$. Also with $J_\phi \approx B_\phi/(qR)$, where q is the rotational transform $q = aB/(RB_\theta)$, then

$$\frac{\Delta\Phi}{\Phi} \approx \frac{a}{qR}\frac{\Delta I}{I} \tag{11}$$

with $qR/a \approx 5$.

V. CORRELATION OF TOROIDAL CURRENT AND VERTICAL DISPLACEMENT ASYMMETRY

The toroidal variation of the current and of the vertical displacement are positively correlated. Fig.5 shows experimental time histories of toroidal current differences $(I_5 - I_1)/I$ plotted as a function of vertical displacement differences $Z_5 - Z_1$, and $(I_7 - I_3)/I$ plotted as a function of $Z_7 - Z_3$, where the subscript refers to toroidal octant. These quantities correspond to $\cos\phi$ and $\sin\phi$ components of I_p, Z_p. Fig.5 also contains simulated $n = 1$ Fourier components I_{cos}/I as a function of ξ_{cos}, and I_{sin}/I as a function of ξ_{sin}, which are the $\cos\phi$ and $\sin\phi$ harmonics of current I and vertical displacement ξ. These quantities are positively correlated, indicating that the toroidal plasma current is higher at toroidal locations where the plasma position is closer to the wall[2,6]. This effect has been explained by invoking skin current at the edge of the plasma[2,10].

It can be shown analytically that the toroidal variation of current and vertical displacement are positively correlated. The maximum current occurs where the vertical displacement is also a maximum. The magnetic field in a large aspect ratio approximation is given by[15]

$$\mathbf{B} = \nabla\psi \times \hat{\phi} + B\hat{\phi} \tag{12}$$

and the displacement is

$$\xi = \nabla\chi \times \hat{\phi}. \tag{13}$$

The magnetic potential ψ is

$$\psi = \psi_0 + \mathbf{B} \cdot \nabla \chi \tag{14}$$

where ψ_0 is the initial poloidal flux, and χ is the displacement potential[6] of the VDE,

$$\chi = \tilde{\chi}_1 + \tilde{\chi}_2, \quad \tilde{\chi}_1 = \chi_1 \cos\theta, \quad \tilde{\chi}_2 = \chi_2 \cos(\theta - \phi) \tag{15}$$

Then ψ can be calculated from (14), (15) as $\psi = \psi_0 + \psi_1 + \psi_2 + \psi_3$ and $\mathbf{B} = \mathbf{B}_0 + \mathbf{B}_1 + \mathbf{B}_2 + \mathbf{B}_3$ with $\mathbf{B}_0 = \nabla\psi_0 \times \hat{\phi} + B\hat{\phi}$, and $\mathbf{B}_k = \nabla\psi_k \times \hat{\phi}$, where $k = 1, 2, 3$. A cylindrical model will be used. The toroidal current is given by

$$I = \oint B_\theta a d\theta = -\oint \psi' d\theta \tag{16}$$

where $I = I_0 + I_1 + I_2 + I_3$, and the prime denotes a radial derivative. Only contributions to ψ that are independent of θ contribute to I. It is also assumed[6] that $\chi = \psi = 0$ at the wall, so that only radial derivatives of χ, ψ will contribute to I.

In zero order, ψ_0 is a function of radius r only. In first, second, and third order,

$$\begin{aligned}
\psi_1 &= \mathbf{B}_0 \cdot \nabla\tilde{\chi}_1 = -\frac{B_{\theta 0}}{a}\chi_1 \sin\theta \\
\psi_2 &= \mathbf{B}_0 \cdot \nabla\tilde{\chi}_2 + \mathbf{B}_1 \cdot \nabla\tilde{\chi}_1 \\
&= -\frac{B_{\theta 0}}{a}\chi_2(1-q)\sin(\theta - \phi) - \frac{B_{\theta 0}}{a^2}\chi_1'\chi_1 \\
\psi_3 &= \mathbf{B}_1 \cdot \nabla\tilde{\chi}_2 + \mathbf{B}_2 \cdot \nabla\tilde{\chi}_1 = -\frac{B_{\theta 0}}{a^2}(\chi_1\chi_2)'(1 - \frac{q}{2})\cos\phi
\end{aligned} \tag{17}$$

and terms with $\sin(2\theta), \cos(2\theta)$ were omitted because they do not contribute to I. The first and second order current vanishes, $I_1 = I_2 = 0$. The asymmetric current is given by

$$\frac{I_3}{2\pi} = -\psi_3' = (2-q)\frac{B_{\theta 0}}{a^2}\chi_1'\chi_2'\cos\phi \tag{18}$$

This is compared to the asymmetric part of the displacement. The displacement in the $\hat{\mathbf{y}}$ direction is given by

$$\xi = \nabla(r\sin\theta) \times \nabla\chi \cdot \hat{\phi} = \xi_1 + \xi_2, \quad \xi_1 = -\frac{1}{2}\chi_1', \quad \xi_2 = -\frac{1}{2}\chi_2'\cos\phi \tag{19}$$

where ξ_1, ξ_2 are the symmetric and asymmetric parts of the vertical displacement, respectively. The symmetric displacement is upward, $\xi_1 > 0$. The asymmetric $\cos\phi$ terms have the ratio

$$\frac{I_3}{\xi_2} = 4(2-q)\frac{I_0\xi_1}{a^2} \tag{20}$$

The ratio of current asymmetry I_3 to the vertical displacement asymmetry ξ_2 is positive, if $q \leq 2$ at the wall.

In the experiment, simulations, and theory, toroidal plasma current is higher at toroidal locations where the plasma position is closer to the wall. There is no need to invoke skin currents[2,10], which are not seen in the M3D simulations, to explain this effect.

VI. NOLL RELATION OF F_x AND M_{IZ}

The Noll relation is used in JET to estimate the asymmetric wall force[19]. The wall force in the wall volume is[3,7]

$$\mathbf{F}_{wall} = \delta_{wall} \oint \oint d\phi dl R \mathbf{J}_{wall} \times \mathbf{B}_{wall} \tag{21}$$

where δ_{wall} is the wall thickness, $\mathbf{J}_{wall}$ is the wall current density, and $\mathbf{B}_{wall}$ is the magnetic field in the wall. The projections of the toroidally varying wall force in the $\hat{\mathbf{x}}, \hat{\mathbf{y}}$ directions are given by $\tilde{F}_x = \mathbf{F} \cdot \hat{\mathbf{x}}, \tilde{F}_y = \mathbf{F} \cdot \hat{\mathbf{y}}$. The magnitude of the asymmetric horizontal force is defined as

$$\Delta F_x = (\tilde{F}_x^2 + \tilde{F}_y^2)^{1/2}. \tag{22}$$

The asymmetric wall force is proportional to the asymmetric vertical current moment, which is given by

$$\Delta F_x \approx \pi B \Delta M_{IZ} \tag{23}$$

where

$$M_{IZ} = \int Z J_\phi d^2 x \tag{24}$$

and the simulated and experimental ΔM_{IZ} are calculated using (4). Fig.6(a) compares the wall force in the simulation with simulated and experimental vertical current moment. The units are in MN. The asymmetric force maximum amplitude is $\Delta F_x = 1.1MN$. The experimental Noll formula predicts a force of $1.3MN$, while the simulated formula predicts $1.2MN$. The agreement is very good. Fig.6(b) shows the peak values in simulations with different values of S_{wall}. The agreement is essentially independent of S_{wall}.

VII. TOROIDAL ROTATION

Asymmetric force rotation is of concern in ITER. Rotation is observed in both experiment and simulations. The rotation angle calculated from the experimental data is

$$\alpha_{exp} = \tan^{-1}\left(\frac{I_5 - I_1}{I_7 - I_3}\right) \tag{25}$$

The simulated rotation angle taken from the current was rather noisy, so the force angle

$$\alpha_{sim} = \tan^{-1}(\frac{\tilde{F}_y}{\tilde{F}_x}) \tag{26}$$

was used instead, where $\tilde{F}_x, \tilde{F}_y$ are defined after (21). Fig.7(a) shows rotation angle α in experiment and in a simulation with $S_{wall} = 10^3$. In both cases there are about $N_{rot} = 2.8$ periods during the CQ time $\tau_{CQ} = 5\tau_{wall}$, which is the time interval of substantial halo current in Fig.1. In runs with $S_{wall} = 250$ and $S_{wall} = 500$, $N_{rot} \approx 2.6$ and $N_{rot} \approx 2.0$ respectively, as shown in Fig.7(b). Also shown in the experimental value $N_{exp} = 2.8$.

Fig.7(b) implies that the rotation frequency is $f_{rot} = N_{rot}/\tau_{CQ} \approx (2S_{wall})^{-1}$. This suggests the rotation is involved with the resistive wall interaction.

VIII. IMPLICATIONS FOR ITER

In the experiment and simulations presented in the previous sections, the maximum wall force occurs after the vertical displacement saturates. In JET, $\tau_{wall}^{JET} = 0.005s$, and the experimental current quench time is $\tau_{CQ}^{JET} \approx 5 \times \tau_{wall} \gg \tau_{wall}$. This will be denoted the high τ_{CQ}/τ_{wall} regime.

There is a second, low τ_{CQ}/τ_{wall} regime, in which $\tau_{CQ}/\tau_{wall} \lesssim 1$, in which the asymmetric wall force and halo current are much smaller. To show this, the wall time was artificially increased, keeping the CQ time fixed. Fig.8 shows JET simulation time histories of I and ξ, with $S_{wall} = 1000$. The subscripts indicate different values of $\tau_{CQ}/\tau_{wall} =$ (a) 1.67, (b) 1.25, (c) 0.83. These were obtained by multiplying τ_{wall}^{JET} in (1), by (a) 3, (b) 4, and (c) 6, noting that in the simulations, $\tau_{CQ}/\tau_{wall} = \tau_{CQ}^{JET}/\tau_{wall}^{JET}$.

There is an interesting crossover in the behavior of ξ. For case (a), ξ saturates in a stationary state, similar to Fig.1. For cases (b),(c), ξ does not saturate, but grows to almost the vertical height of the wall. Saturation of ξ seems to require $\tau_{CQ}/\tau_{wall} \gtrsim 1.5$. It is also noteworthy that a faster CQ causes a speedup of the VDE.

In Fig.9(a),(b), the ratio τ_{CQ}/τ_{wall} was varied by replacing the experimental wall time in (1) by a wider range of values, $0.005 \leq \tau_{wall}^{JET} \leq 0.03$. The cases in Fig.8 have the smallest τ_{CQ}/τ_{wall} and ΔF_x values in Fig.9(a). From Fig.8 and Fig.9(a) it is possible to distinguish three regimes of τ_{CQ}/τ_{wall}. In the low τ_{CQ}/τ_{wall} regime $\tau_{CQ}/\tau_{wall} \lesssim 1.5$, the asymmetric wall force is small, while in the high τ_{CQ}/τ_{wall} regime $\tau_{CQ}/\tau_{wall} \gtrsim 4$, ΔF_x is large. There is also an intermediate regime $1.5 \lesssim \tau_{CQ}/\tau_{wall} \lesssim 4$.

A reason for this behavior is that a large force seems to require both a large vertical displacement and a large current. Fig.6(a) shows that the asymmetric wall force ΔF_x is maximum when ξ and I are simultaneously near their maximum values in Fig.1. Fig.8 shows that in the low τ_{CQ}/τ_{wall} regime ξ and I do not simultaneously have their largest values.

The fit in Fig.9(a) is to

$$\Delta F_x = c_1[1 + \tanh(c_2\frac{\tau_{CQ}}{\tau_{wall}} - c_3)] \tag{27}$$

where $c_1 = 1.1, c_2 = 1$, and $c_3 = 2.7$. The half maximum occurs when $\tau_{CQ}/\tau_{wall} \approx 2.7$.

Fig.9(a) also shows the dependence of the Noll formula (23) on τ_{CQ}/τ_{wall}. It is in agreement with ΔF_x, in the high τ_{CQ}/τ_{wall} regime, but otherwise greatly exceeds the wall force. It suggests that (23) gives an upper limit to the asymmetric wall force. Here the fit is to (27) with $\pi B \Delta M_{IZ}$ replacing ΔF_x, $c_1 = 1.2$, $c_2 = 0.9$, and $c_3 = 1.9$.

Fig.9(b) shows the simulated toroidally averaged halo current HF and the toroidally varying halo current ΔHF defined in (5) as a function of τ_{CQ}/τ_{wall}, as in Fig.9(b). The fits are to HF, ΔHF on the left side of (27), with $c_1 = 0.17, c_2 = 0.85, c_3 = 1.3$, and $c_1 = 0.07, c_2 = 1, c_3 = 3$ respectively. A related ITER study[14] found that reducing τ_{CQ} by mitigation reduced the halo current, by causing a CQ before the vertical displacement was large.

The low τ_{CQ}/τ_{wall} regime is the regime most relevant to ITER. The ITER wall time is much longer than in JET. The walls in ITER[22] have thickness $\delta = 6cm$, resistivity $\eta = 0.825\mu\Omega m$, and minor radius of the inner wall in the poloidal midplane $a_1 = 1.35 \times a_p = 2.7m$

where $a_p = 2m$ is the plasma minor radius. This gives the wall time $\tau_{wall}^{ITER} = \mu_0 a_1 \delta/\eta =$ $0.26s$. A mitigated CQ time might be $0.05s - 0.15s$[9,23,24]. In a slow unmitigated ITER CQ, $\tau_{CQ} \lesssim 0.3s$[24]. In these examples, $\tau_{CQ}^{ITER} \leq \tau_{wall}^{ITER}$. There might be slow[24] CQs with $\tau_{CQ}^{ITER} \lesssim 0.6s$.

It has been predicted that the asymmetric wall force in ITER might be 25 times as large as the wall force in JET[2], which is a serious concern in the high τ_{CQ}/τ_{wall} regime.

The simulations suggest that the wall force in ITER will be much less in the low τ_{CQ}/τ_{wall} regime. If the wall force in the low τ_{CQ}/τ_{wall} regime is 4% of the maximum, then the scaling to ITER is $25 \times 0.04 = 1$, so that ΔF_x might be the same in ITER as in JET.

Previous simulations of ITER disruptions[3,4] found a large variation in the amplitude of ΔF_x which depended on τ_{wall}. In some of the simulations[4], a VDE caused magnetic flux to be scraped off, so that the last closed flux surface had $q = 2$. This caused a 3D MHD instability with growth rate γ, which produced a maximum asymmetric force if it saturated in about the wall time, $\gamma\tau_{wall} = \mathcal{O}(1)$. When the wall time was larger, $\gamma\tau_{wall} \ll 1$, the amplitude of asymmetric wall force was an order of magnitude less. Other simulations[4] modeled the effect of massive gas injection by concentrating the current within the $q = 2$ surface. As in the present simulations, the 3D MHD instability was present before the VDE. An example was given in the low τ_{CQ}/τ_{wall} regime, with ΔF_x less than 10% of the maximum value. In those previous simulations, the CQ was not controlled, and the scaling of ΔF_x with τ_{CQ}/τ_{wall} was not studied systematically.

In order to confirm that the JET results in the low τ_{CQ}/τ_{wall} regime are applicable to ITER, it is important to perform simulations with ITER geometry and parameters, with control of the CQ, as in the present study. It is important to see if ITER is similar to cases (b), (c), in Fig.8, which have wall force much smaller than the maximum value, as shown in Fig.9(a).

IX. SUMMARY

Nonlinear 3D MHD asymmetric vertical displacement disruptions simulations have been performed using JET equilibrium reconstruction initial data. Several experimentally measured quantities were compared with the simulation. It was found that there was reasonable agreement between simulation and experiment. The quantities that were compared were the VDE displacement and toroidal current, the halo current, the toroidal current asymmetry, and toroidal rotation. The experimental data and the simulations are in reasonable agreement. The toroidal current and vertical displacement asymmetry are positively correlated as in the experiment. It is not necessary to invoke skin current to explain the correlation. The Noll relation between asymmetric wall force and vertical current moment is verified in the simulations. Also verified is toroidal variation of toroidal magnetic flux. An important feature of the simulations is that most of the quantities are independent of S_{wall}, when the time is also scaled to S_{wall}. This allows simulations to be run for much shorter times than when the experimental S_{wall} is used. The values of the compared quantities in this JET shot are fairly typical of JET disruption data. In future work other experimental shots might be compared to simulations.

In JET, the wall time is much less than the current quench time, $\tau_{wall} \ll \tau_{CQ}$, which is the high τ_{CQ}/τ_{wall} regime. It was shown in JET simulations that there is also a low τ_{CQ}/τ_{wall} regime, in which $\tau_{wall} \gtrsim \tau_{CQ}$. In this regime the asymmetric wall force and halo current are much less than in the slow CQ regime. The low τ_{CQ}/τ_{wall} regime is more relevant to ITER. Extrapolating from JET data might greatly overestimate the expected ITER asymmetric wall force. It is important to carry out further ITER simulations to verify this conclusion.

Acknowledgement: We thank M. Lehnen for helpful comments. This research was supported by USDOE, has been carried out within the framework of the EUROfusion Consortium, and has received funding from the Euratom research and training programme 2014-2018 under grant agreement No 633053. The views and opinions expressed herein do not necessarily reflect those of the European Commission.

REFERENCES

[1] T. Hender, J. C. Wesley, J. Bialek, A. Bondeson, A. Boozer, R. J. Buttery, A. Garofalo, T. P Goodman, R. S. Granetz, Y. Gribov, O. Gruber, M. Gryaznevich, G. Giruzzi, S. Günter, N. Hayashi, P. Helander, C. C. Hegna, D. F. Howell, D. A. Humphreys, G. T. A. Huysmans, A. W.

Hyatt, A. Isayama, S. C. Jardin, Y. Kawano, A. Kellman, C. Kessel, H. R. Koslowski, R. J. La Haye, E. Lazzaro, Y. Q. Liu, V. Lukash, J. Manickam, S. Medvedev, V. Mertens, S. V. Mirnov, Y. Nakamura, G. Navratil, M. Okabayashi, T. Ozeki, R. Paccagnella, G. Pautasso, F. Porcelli, V. D. Pustovitov, V. Riccardo, M. Sato, O. Sauter, M. J. Schaffer, M. Shimada, P. Sonato, E. J. Strait, M. Sugihara, M. Takechi, A. D. Turnbull, E. Westerhof, D. G. Whyte, R. Yoshino, H. Zohm and the ITPA MHD, Disruption and Magnetic Control Topical Group, Nuclear Fusion **47** S128 - 202 (2007). Progess in the ITER Physics Basis Chapter 3: MHD Stability, operational limits and disruptions, Nuclear Fusion **47** (2007) S128 - S202.

[2]S.N. Gerasimov, T.C. Hender, J. Morris, V. Riccardo, L.E. Zakharov and JET EFDA Contributors, Plasma current asymmetries during disruptions in JET, Nucl. Fusion **54** 073009 (2014).

[3]H. R. Strauss, R. Paccagnella, J. Breslau, Wall forces produced during ITER disruptions, Phys. Plasmas (2010) **17**, 082505.

[4]H. Strauss, R. Paccagnella, J. Breslau, L. Sugiyama, S. Jardin, Sideways Wall Force Produced During Disruptions, Nucl. Fusion **53**, 073018 (2013).

[5]H. R. Strauss, L. Sugiyama, R. Paccagnella, J. Breslau, S. Jardin, Tokamak toroidal rotation caused by AVDEs and ELMs, Nuclear Fusion **54**, 043017 (2014).

[6]H. Strauss, Toroidal current asymmetry in tokamak disruptions, Physics of Plasmas **21**, 102509 (2014).

[7]H. Strauss, Asymmetric Wall Force and Toroidal Rotation in Tokamak Disruptions, Phys. Plasmas **22**, 082509 (2015)

[8]V. A. Izzo, D. G. Whyte, R. S. Granetz, P. B. Parks, E. M. Hollmann, L. L. Lao, J. C. Wesley, Magnetohydrodynamic simulations of massive gas injection int Alcator C - Mod and DIII-D plasmas, Phys. Plasmas **15**, 056109 (2008).

[9]E. M. Hollmann, P. B. Aleynikov, T. Flp, D. A. Humphreys, V. A. Izzo, M. Lehnen, V. E. Lukash, G. Papp, G. Pautasso, F. Saint-Laurent, and J. A. Snipes, Status of research toward the ITER disruption mitigation system, Phys. Plasmas **22**, 021802 (2015).

[10]L. E. Zakharov, The theory of the kink mode during the vertical plasma disruption events in tokamaks, Phys. Plasmas **15** 062507 (2008).

[11]L. E. Zakharov, Sergei A. Galkin, Sergei N. Gerasimov, and JET-EFDA contributors, Understanding disruptions in tokamaks, Phys. Plasmas **19** 055703 (2012).

[12]R. Roccella, M. Roccella, V. Riccardo, S. Chiocchio and JET Contributors, Asymmetric toroidal eddy currents (ATEC) to explain sideways forces at JET Nuclear Fusion **56** 106010 (2016).

[13]R. R. Khayrutdinov, V. E. Lukash, V. D. Pustovitov, Local and integral forces on the vacuum vessel during thermal quench in the ITER tokamak Plasma Physics and Controlled Fusion **58** 115012 (2016).

[14]M. Sugihara, S. Putvinski, D. J. Campbell, S. Carpentier-Chouchana, F. Escourbiac, S. Gerasimov, Yu. Gribov, T. C. Hender, T. Hirai, K. Ioki, R. Khayrutdinov, H. Labidi, V. Lukash, S. Maruyama, M. Merola, R. Mitteau, S. Miyamoto, J. Morris, G. Pautasso, R. A. Pitts, R. Raffray, V. Riccardo, R. Roccella, G. Sannazzaro, T. Schioler, J. Snipes, R. Yoshino Disruption Impacts and Their Mitigation Target Values for ITER Operation and Machine Protection, ITR/P1-14, IAEA Fusion Energy Conference 2012, San Diego.

[15]W. Park, E. Belova, G. Y. Fu, X. Tang, H. R. Strauss, L. E. Sugiyama, Plasma Simulation Studies using Multilevel Physics Models, Phys. Plasmas **6** 1796 (1999).

[16]S. N. Gerasimov, P. Abreu, M. Baruzzo, V. Drozdov, A. Dvornova, J. Havlicek, T.C. Hender, O. Hronova, U. Kruezi1, X. Li, T. Markovi, R. Pnek, G. Rubinacci, M. Tsalas, S. Ventre, F. Villone, L.E. Zakharov and JET Contributorsa JET and COMPASS asymmetrical disruptions, Nucl. Fusion **55** 113006 (2015).

[17]V. Riccardo, G. Arnoux, P. Cahyna, T. C. Hender, A. Huber, S. Jachmich, V. Kiptily, R. Koslowski, L. Krlin, M. Lehnen, A. Loarte, E. Nardon, R. Paprok, D. Tskhakaya (Sr) and JET-EFDA contributors JET disruption studies in support of ITER, Plasma Phys. Contr. Fusion **52**, (2010).

[18]P. Noll, P. Andrew, M. Buzio, R. Litunovski, T. Raimondi, V. Riccardo, and M. Verrecchia, (Proc. 19th Symposium on Fusion Technology, Lisbon, 1996) ed. C. Varandas and F. Serra (Elsevier, Amsterdam, 1996), Vol. 1, p. 751.

[19]V. Riccardo, P. Noll, S.P. Walker, Forces between plasma, vessel and TF coils during AVDEs at JET, Nuclear Fusion **40** 1805 (2000).

[20]V. Riccardo, T. C. Hender, P. J. Lomas, B. Alper, T. Bolzonella, P. de Vries, G. P. Maddison and the JET EFDA Contributors, Analysis of JET halo currents, Plasma Phys. Control. Fusion **46**, 925 (2004).

[21]R. Albanese, M. Mattei and F. Villone, Prediction of the growth rates of VDEs in JET, Nucl. Fusion **44**, 999 (2004).

[22]Y. Gribov and V. D. Pustovitov, Analytical study of RWM feedback stabilisation with application to ITER, Proc. 19th IAEA Fusion Energy Conf. (Lyon, 2002) CT/P-12 http://www-pub.iaea.org/MTCD/publications/PDF/csp_019c/pdf/ctp_12.pdf

[23]M. Lehnen, Physics basis for ITER disruption mitigation gaps and present R&D, Theory and Simulation of Disruptions Workshop, Princeton, 20 July 2016, http://tsdw.pppl.gov/Talks/2016/Lehnen.pdf

[24]D. Kiramov, M. Lehnen, R. Khayrutdinov, V., Lukash, ITER disruption simulations with improved power balance in the halo region, 43rd EPS Conference on Plasma Physics, P4.071 (2016), http://ocs.ciemat.es/EPS2016PAP/pdf/P4.071.pdf

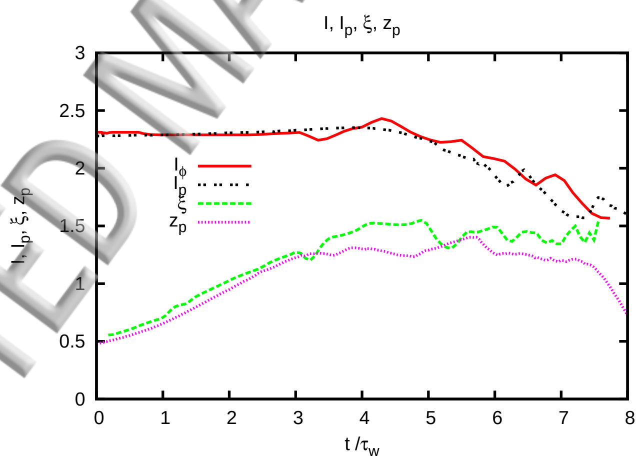

FIG. 1. Time history plot of simulated toroidal current I, experimental toroidal current I_p, simulated vertical displacement ξ, and experimental vertical displacement z_p. Simulation quantities are in time units $\tau_{wall} = S_{wall}\tau_A$, with $S_{wall} = 1000$. Experimental quantities are in time units τ_{wall}^{JET}.

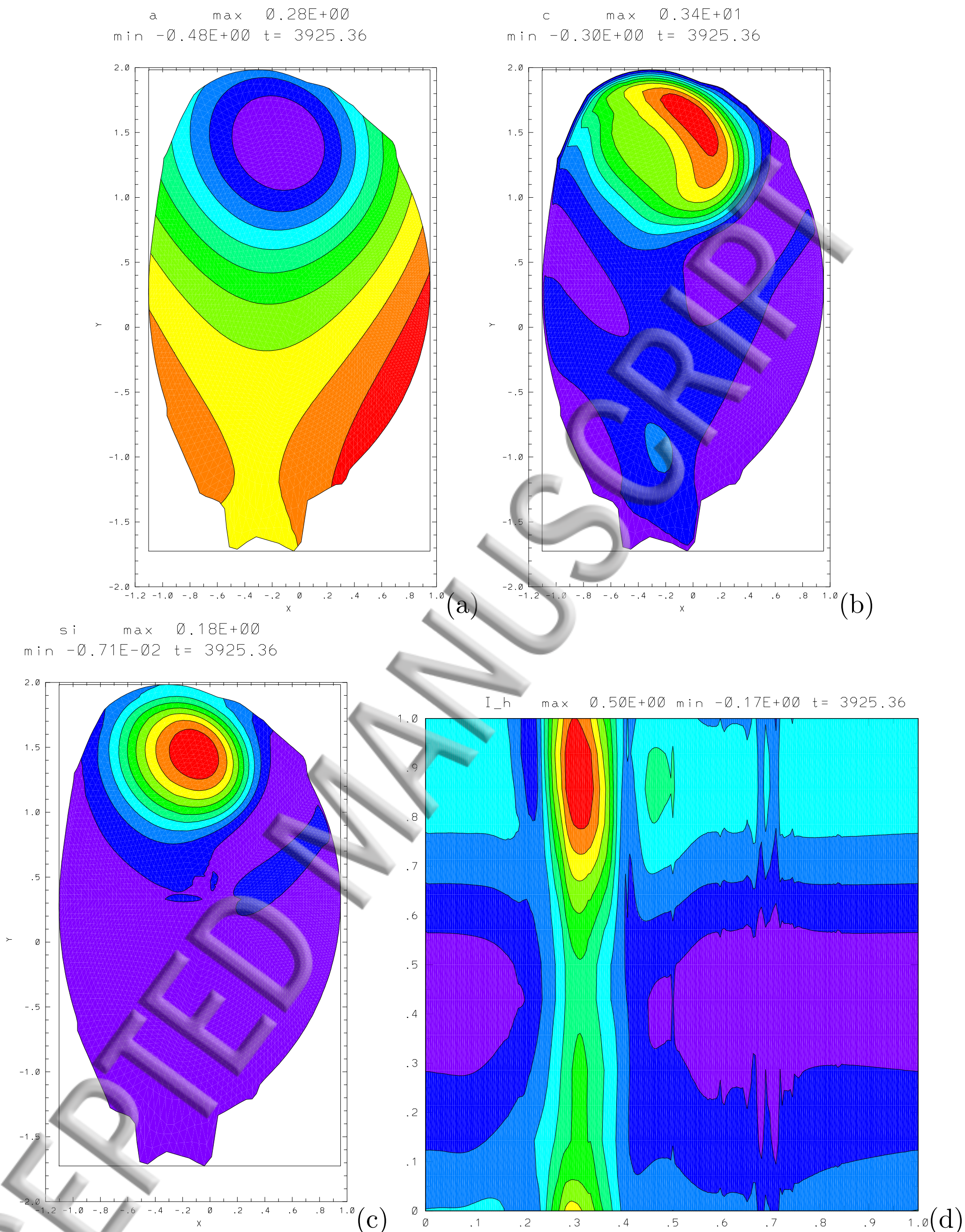

FIG. 2. (a) Contour plot of poloidal magnetic flux ψ at time $t = 3.93\tau_{wall}$ in the (R, Z) plane with $\phi = 0$, with $S_{wall} = 1000$, when the vertical displacement has saturated. (b) Contours of toroidal current at the same time. A large $(m, n) = (1, 1)$ mode is present. (c) Contours of toroidal magnetic flux RB_ϕ. (d) Perturbed toroidal field on the wall, $R\delta B_\phi$ at the same time. The vertical coordinate is the toroidal angle $\phi/(2\pi)$, and the horizontal coordinate is a poloidal angle $\theta/2\pi$.

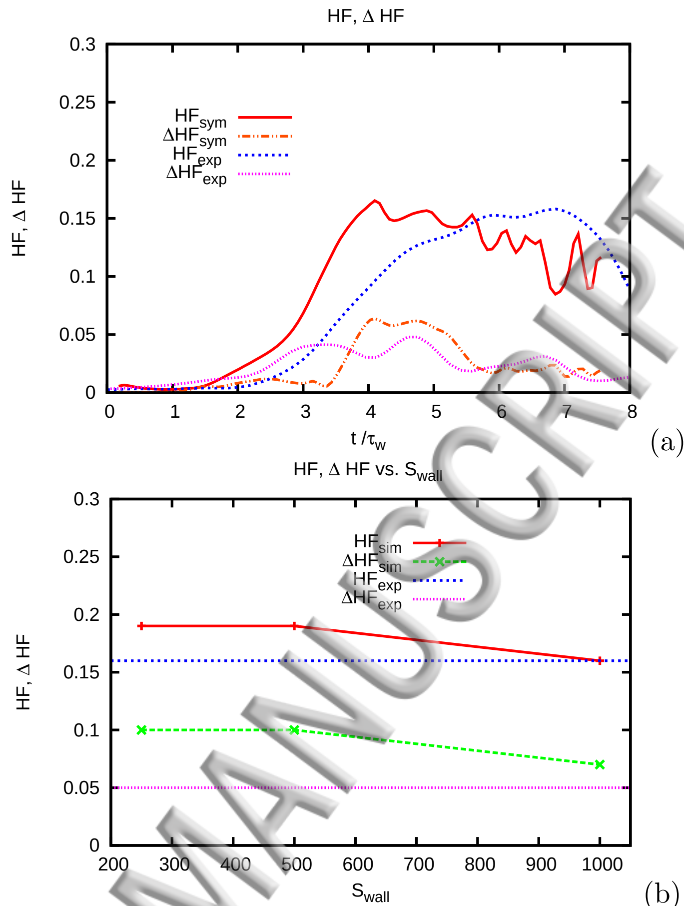

FIG. 3. (a) Time history of toroidally averaged experimental halo current HF_{exp}, toroidally varying experimental halo current ΔHF_{exp}, toroidally averaged simulated halo current HF_{sim}, and toroidally varying simulated halo current ΔHF_{sim}, defined in (5) with simulation $S_{wall} = 1000$. (b) Maximum values in time of toroidally averaged HF and varying ΔHF, both simulated and experimental, as a function of S_{wall}.

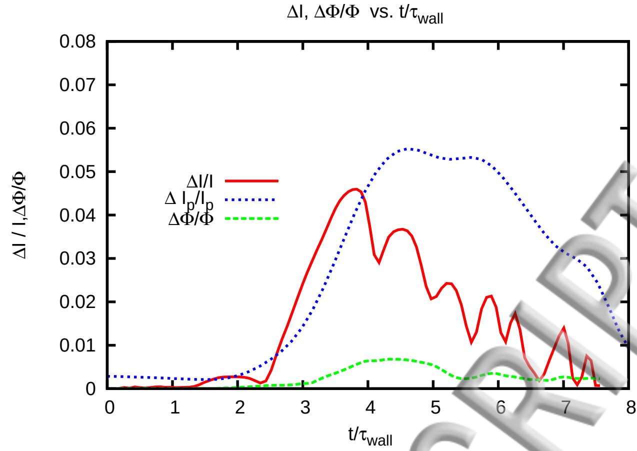

FIG. 4. Time history plot shows magnitude of toroidal current variation comparing JET data $\Delta I_p/I_p$ and simulation $\Delta I/I$. Also shown is the toroidally varying toroidal flux amplitude $\Delta\Phi/\Phi$.

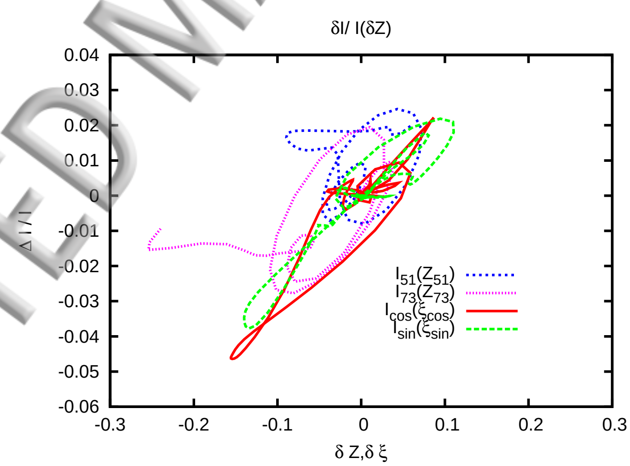

FIG. 5. Time history of toroidal current differences $\delta I/I$ as a function of vertical displacement differences $\delta\xi, \delta z_p$, in experiment and simulation.

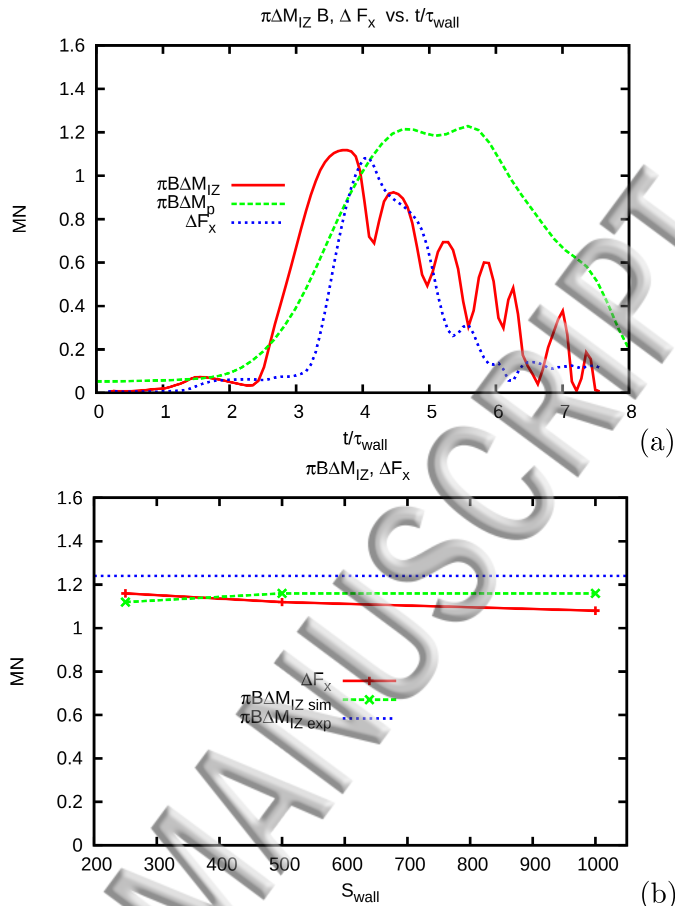

FIG. 6. (a) Simulated asymmetric wall force ΔF_x is consistent with the Noll formula, which is calculated both from the simulation ΔM_{IZsim} and the experimental data ΔM_{IZexp}. (b) Peak values are in agreement, essentially independent of S_{wall}. The units are MN.

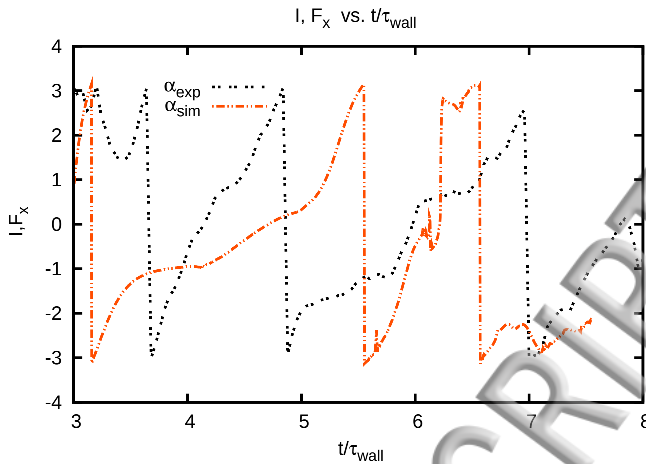

(a)

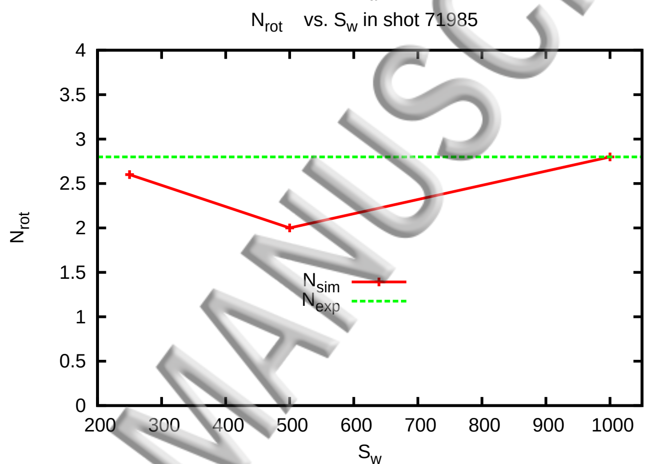

(b)

FIG. 7. Rotation of toroidal current and wall force. (a) wall force angle in wall time units, for $S_{wall} = 10^3$. Also shown is the experimental current rotation angle. (b) Rotation number $N_{rot} = (\alpha_F - \alpha_i)/(2\pi)$ as a function of S_{wall}. Also shown is the experimental value of N_{rot} taken from Fig.7(a).

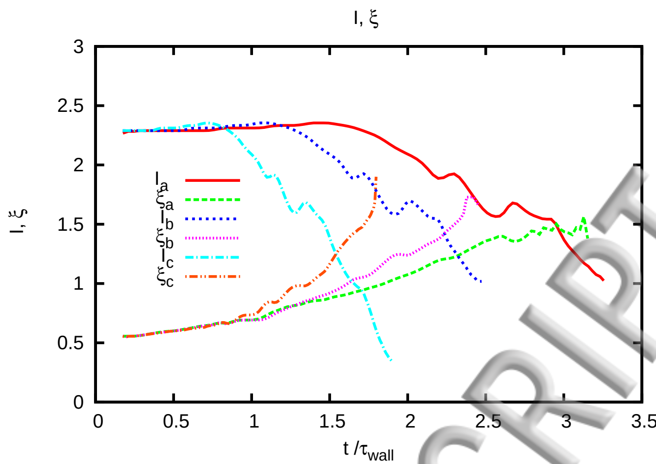

FIG. 8. Time histories of I, ξ as in Fig.1, with $S_{wall} = 1000$. Subscipts denote values of $\tau_{CQ}/\tau_{wall} =$ (a) 1.67, (b) 1.25, (c) 0.83. In case (a) ξ saturates in a steady state, while in (b) , (c) ξ does not saturate.

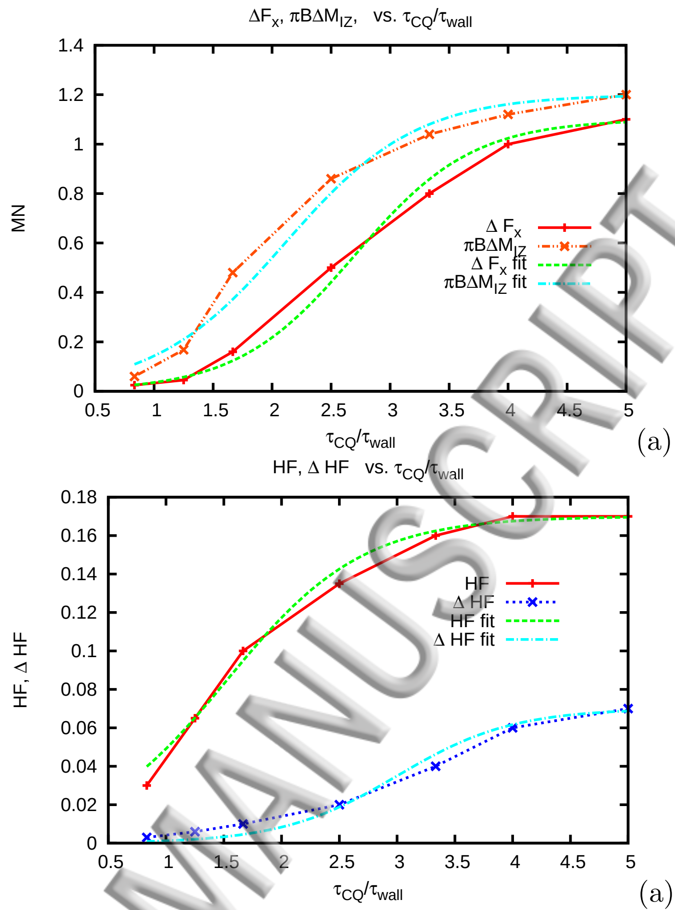

FIG. 9. (a) Peak ΔF_x and $\pi B \Delta M_{IZ}$ as a function of τ_{CQ}/τ_{wall}, with fitting functions. (c) Peak halo fractions HF, ΔHF as a function of τ_{CQ}/τ_{wall}, with fit.

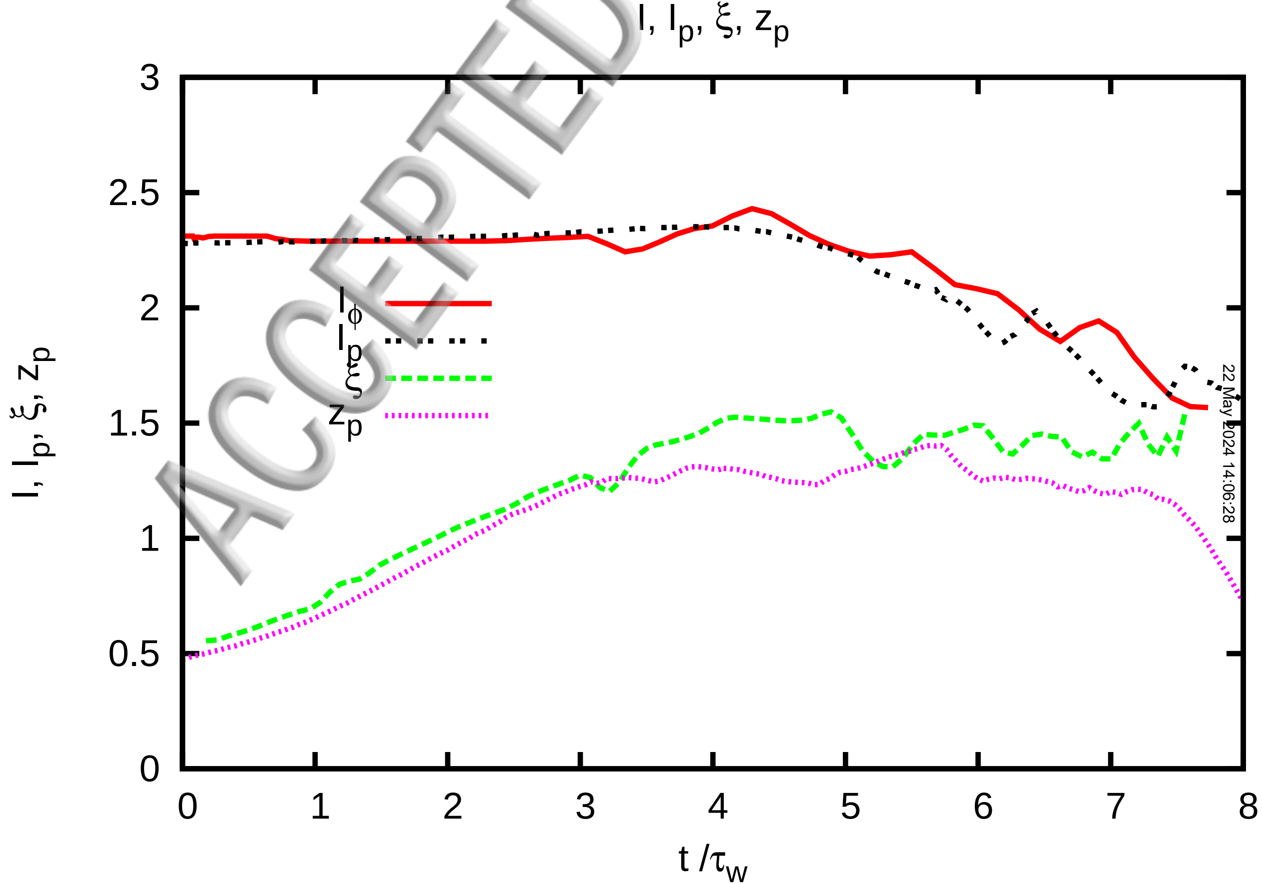

I, I_p, ξ, z_p
I_φ
I_p
ξ
z_p
3
2.5
2
1.5
1
0.5
0
0
1
2
3
4
5
6
7
8
t /τ_w
I, I_p, ξ, z_p

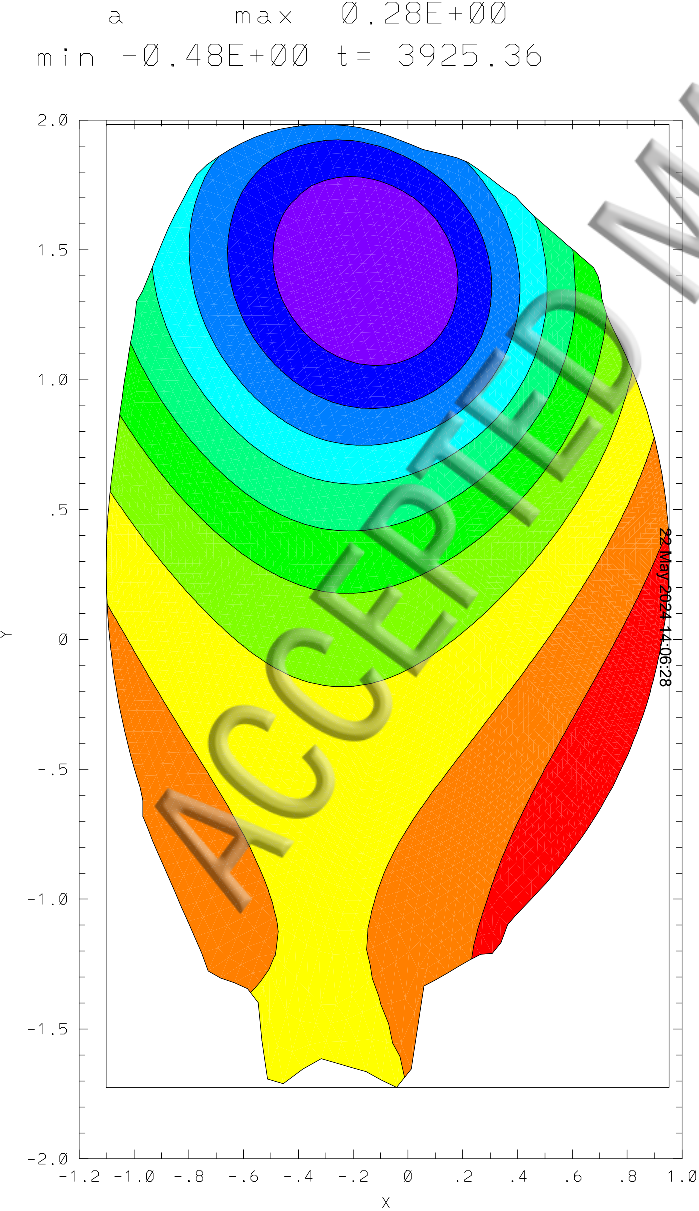
a max Ø.28E+ØØ
min -Ø.48E+ØØ t= 3925.36
2.Ø
1.5
1.Ø
.5
Ø
-.5
-1.Ø
-1.5
-2.Ø
Y
-1.2
-1.Ø
-.8
-.6
-.4
-.2
Ø
.2
.4
.6
.8
1.Ø
X
22 May 2024 14:06:28

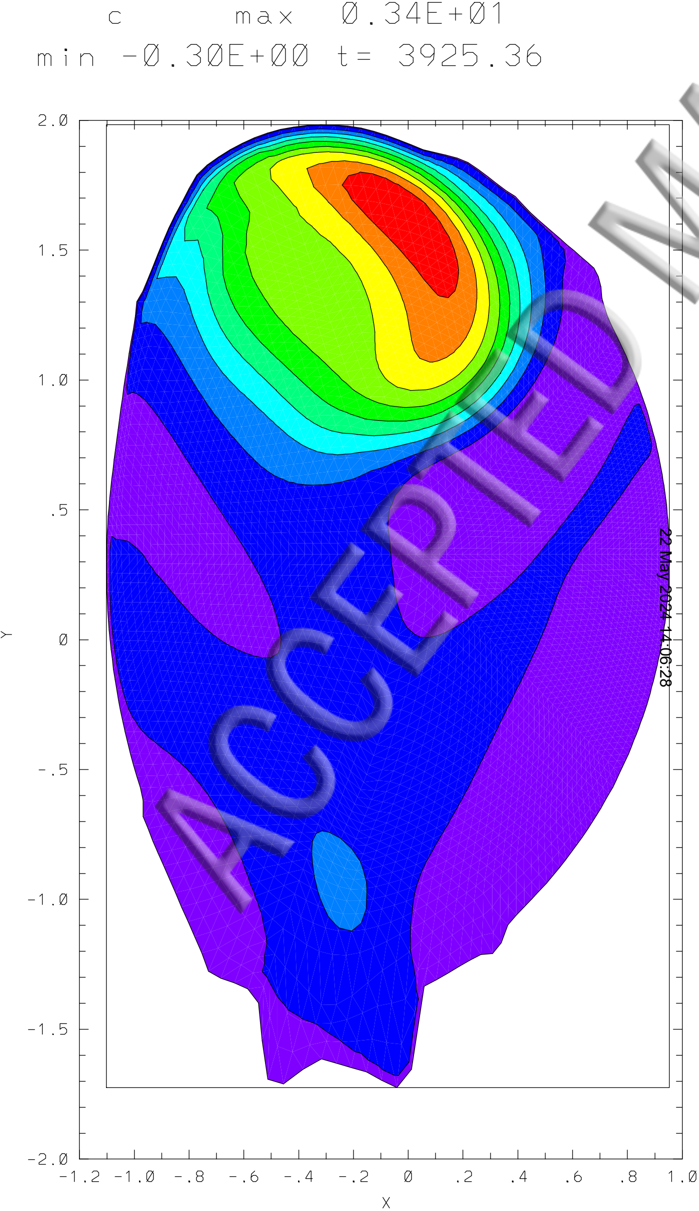
c max 0.34E+01
min -0.30E+00 t= 3925.36
2.0
1.5
1.0
.5
0
-.5
-1.0
-1.5
-2.0
Y
-1.2
-1.0
-.8
-.6
-.4
-.2
0
.2
.4
.6
.8
1.0
X
22 May 2024 14:06:28

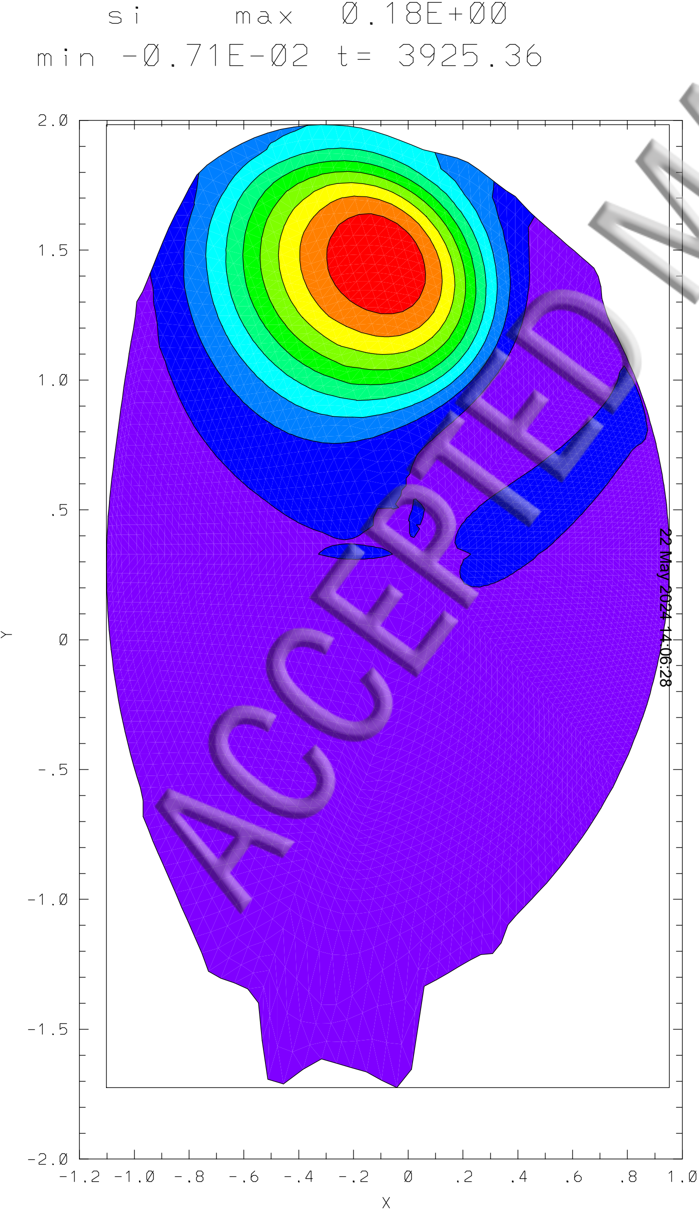
si max 0.18E+00
min -0.71E-02 t= 3925.36
2.0
1.5
1.0
.5
0
-.5
-1.0
-1.5
-2.0
Y
-1.2
-1.0
-.8
-.6
-.4
-.2
0
.2
.4
.6
.8
1.0
X
22 May 2024 14:06:28
ACCEPTED

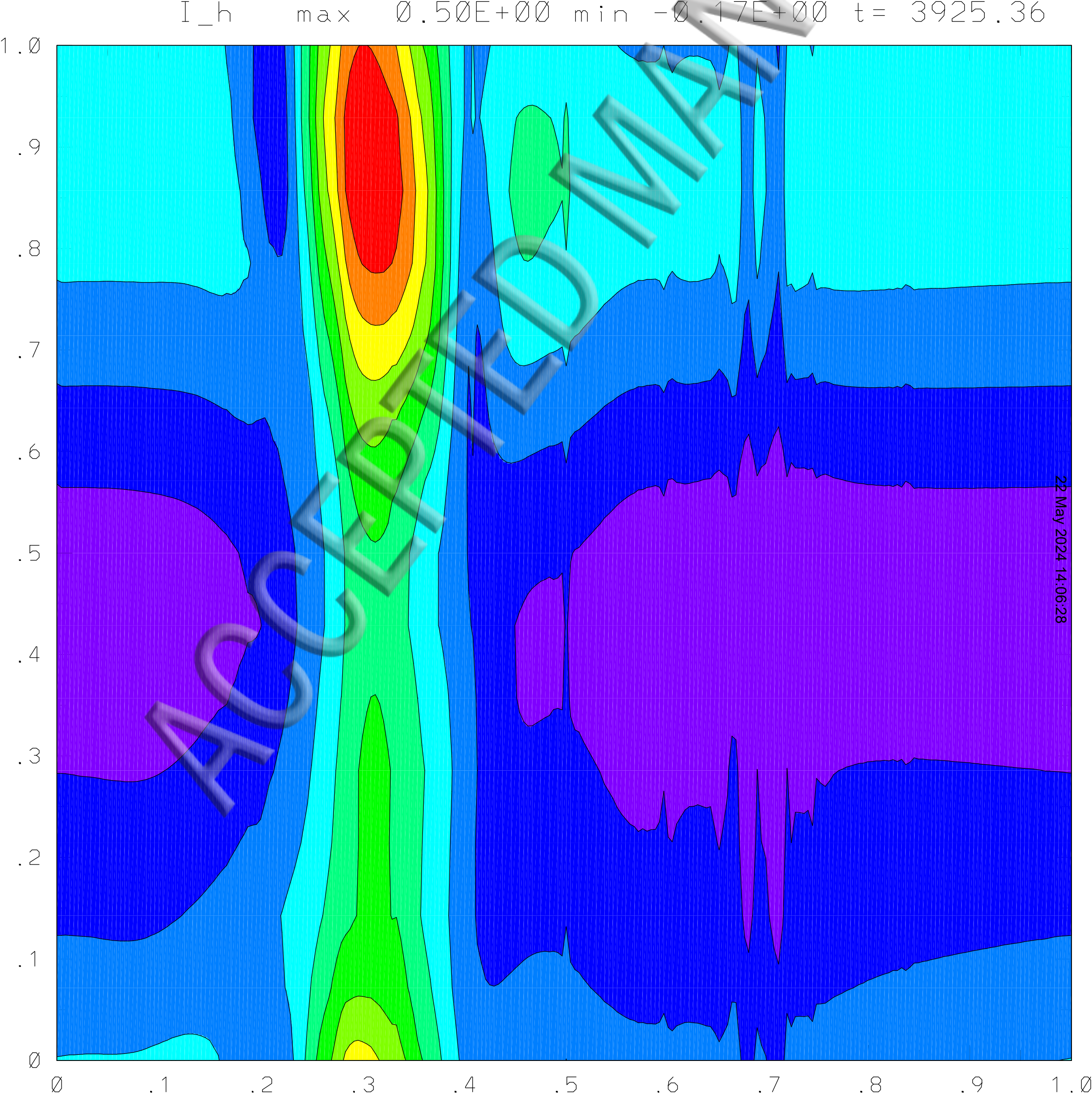
I_h max 0.50E+00 min -0.17E+00 t= 3925.36
1.0
.9
.8
.7
.6
.5
.4
.3
.2
.1
0
0
.1
.2
.3
.4
.5
.6
.7
.8
.9
1.0
22 May 2024 14:06:28

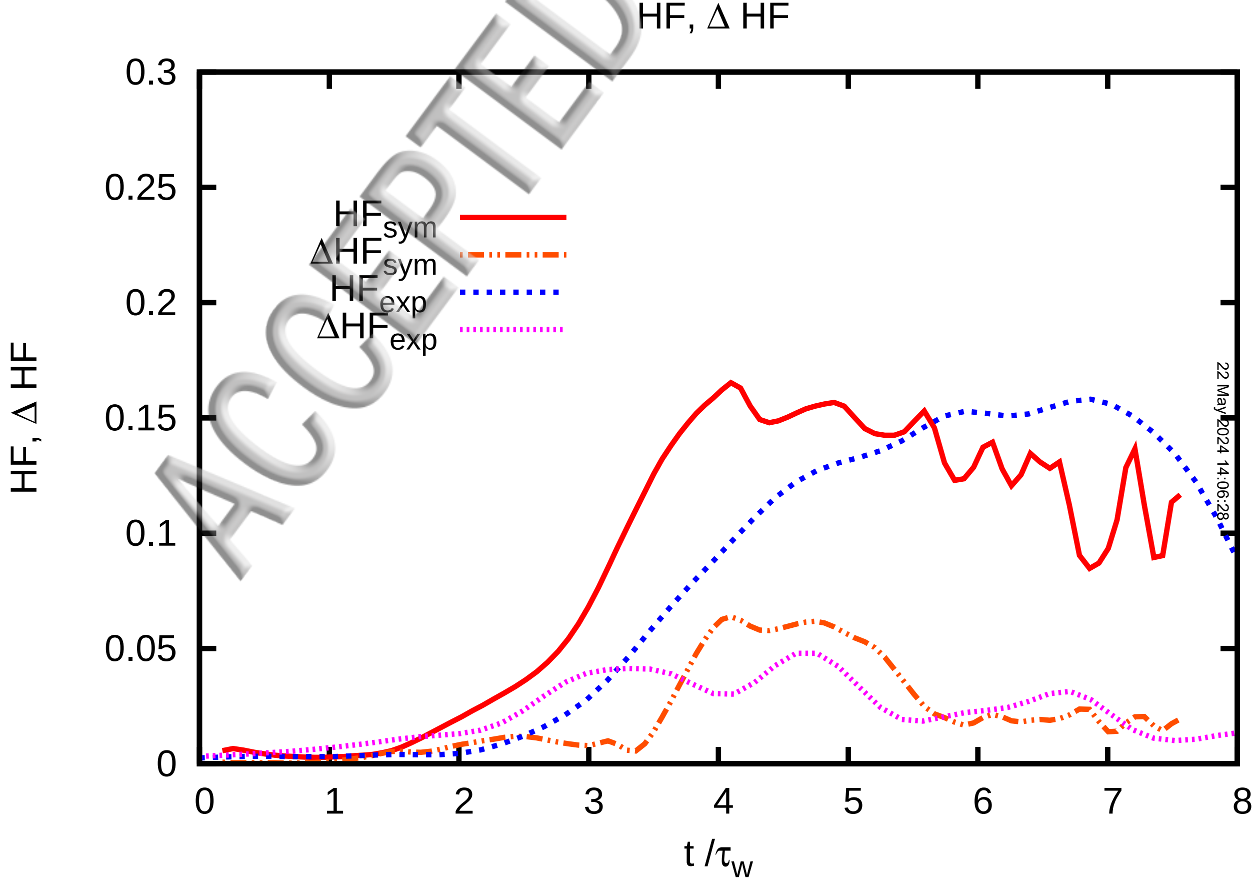
HF, Δ HF
HF_{sym}
ΔHF_{sym}
HF_{exp}
ΔHF_{exp}
0.3
0.25
0.2
0.15
0.1
0.05
0
0 1 2 3 4 5 6 7 8
t /τ_w
HF, Δ HF
22 May 2024 14:06:28

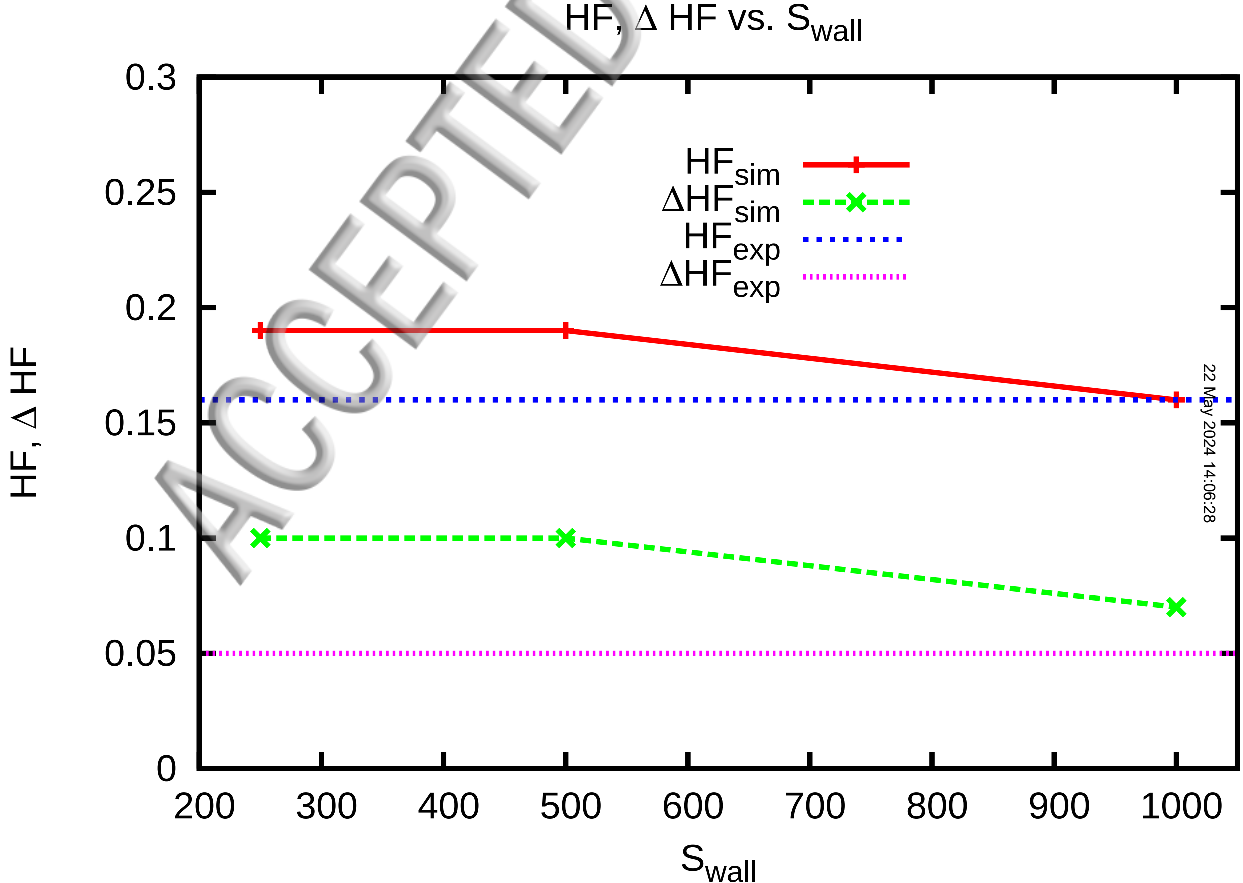
HF, Δ HF vs. S_wall
HF_sim
ΔHF_sim
HF_exp
ΔHF_exp
HF, Δ HF
S_wall
0
0.05
0.1
0.15
0.2
0.25
0.3
200
300
400
500
600
700
800
900
1000
ACCEPTED
22 May 2024 14:06:28

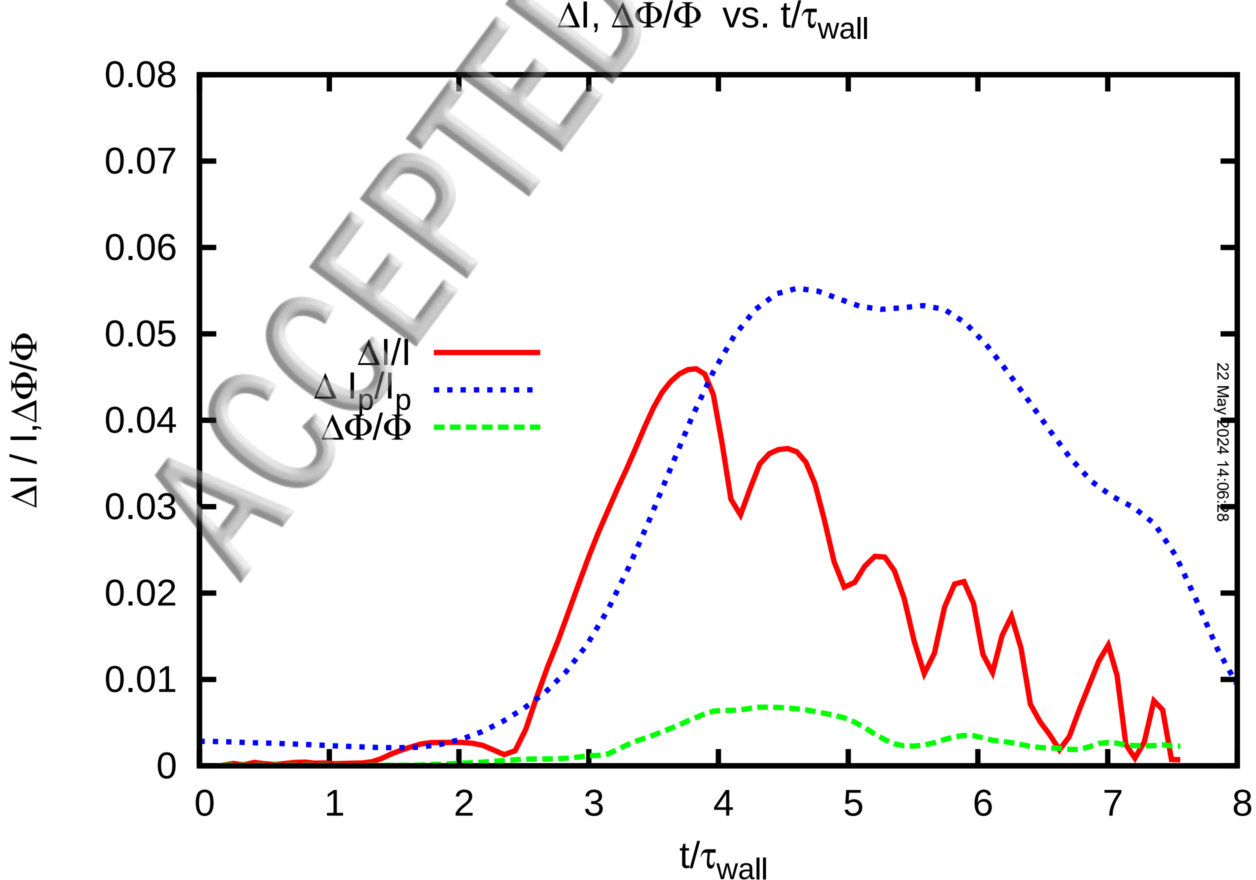

ΔI, ΔΦ/Φ vs. t/τwall
0.08
0.07
0.06
0.05
0.04
0.03
0.02
0.01
0
0
1
2
3
4
5
6
7
8
t/τwall
ΔI / I,ΔΦ/Φ
ΔI/I
Δ Ip/Ip
ΔΦ/Φ
22 May 2024 14:06:18

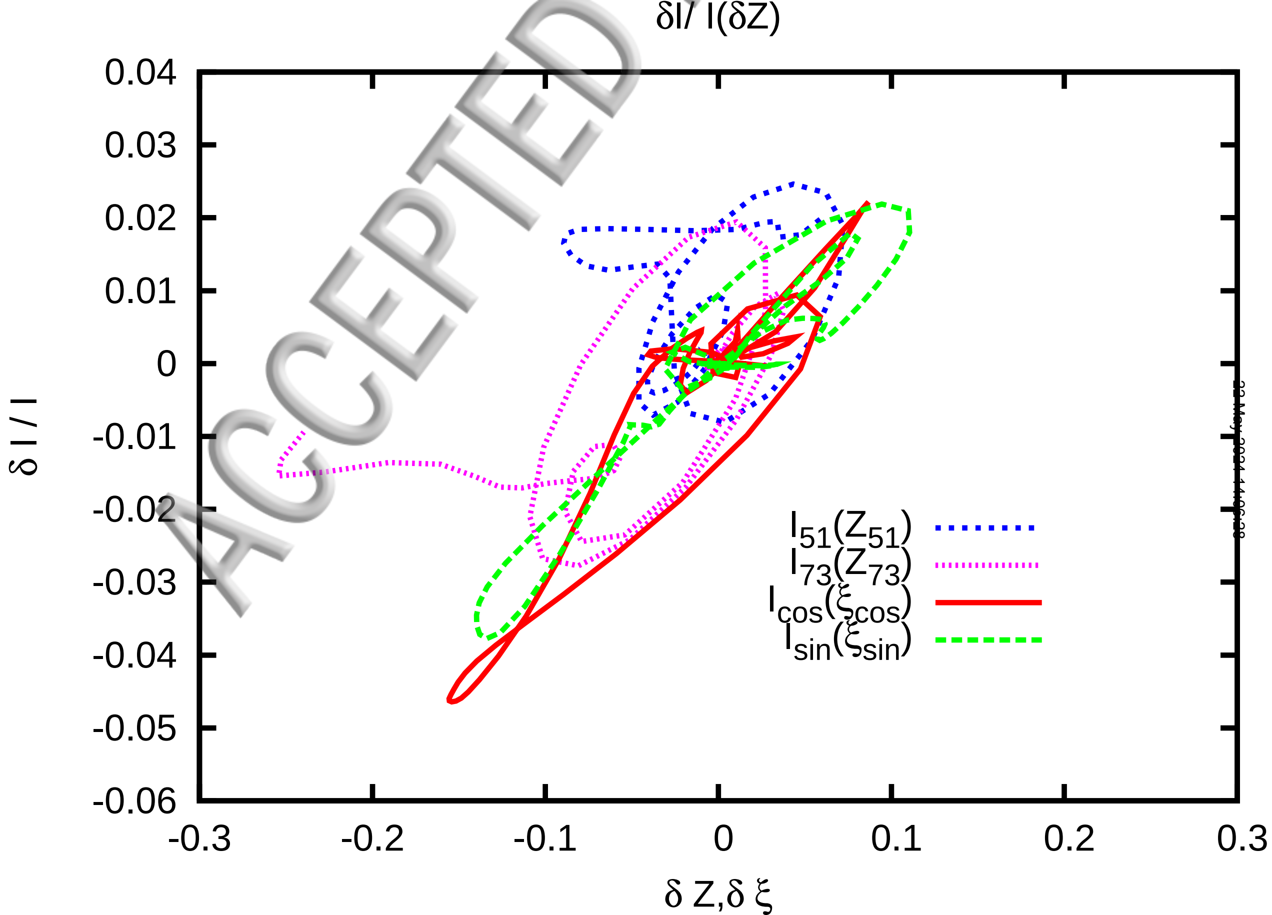

δI/ I(δZ)
δ I / I
δ Z,δ ξ
0.04
0.03
0.02
0.01
0
-0.01
-0.02
-0.03
-0.04
-0.05
-0.06
-0.3
-0.2
-0.1
0
0.1
0.2
0.3
I51(Z51)
I73(Z73)
Icos(ξcos)
Isin(ξsin)
ACCEPTED

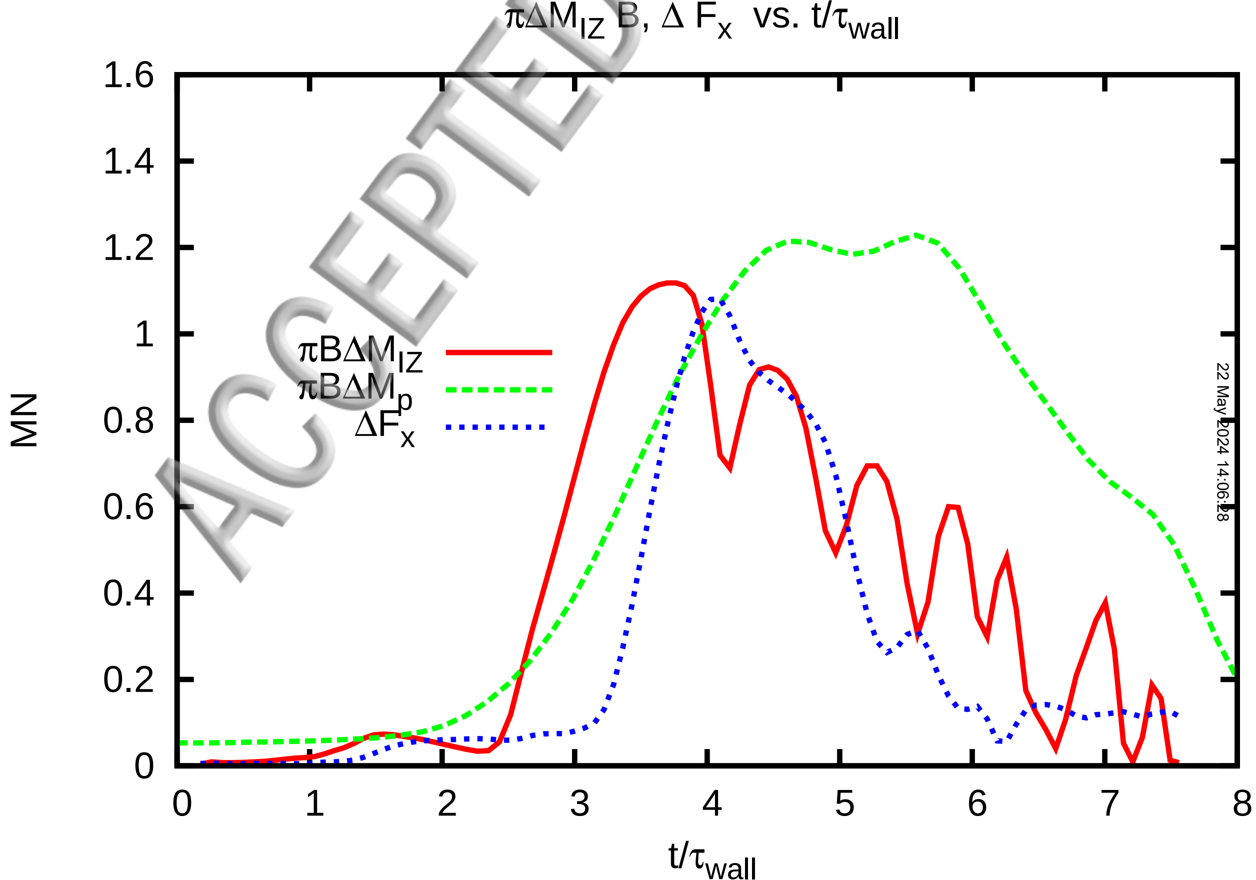
πΔM_IZ B, Δ F_x vs. t/τ_wall
1.6
1.4
1.2
1
0.8
0.6
0.4
0.2
0
MN
πBΔM_IZ
πBΔM_p
ΔF_x
0
1
2
3
4
5
6
7
8
t/τ_wall
22 May 2024 14:06:18

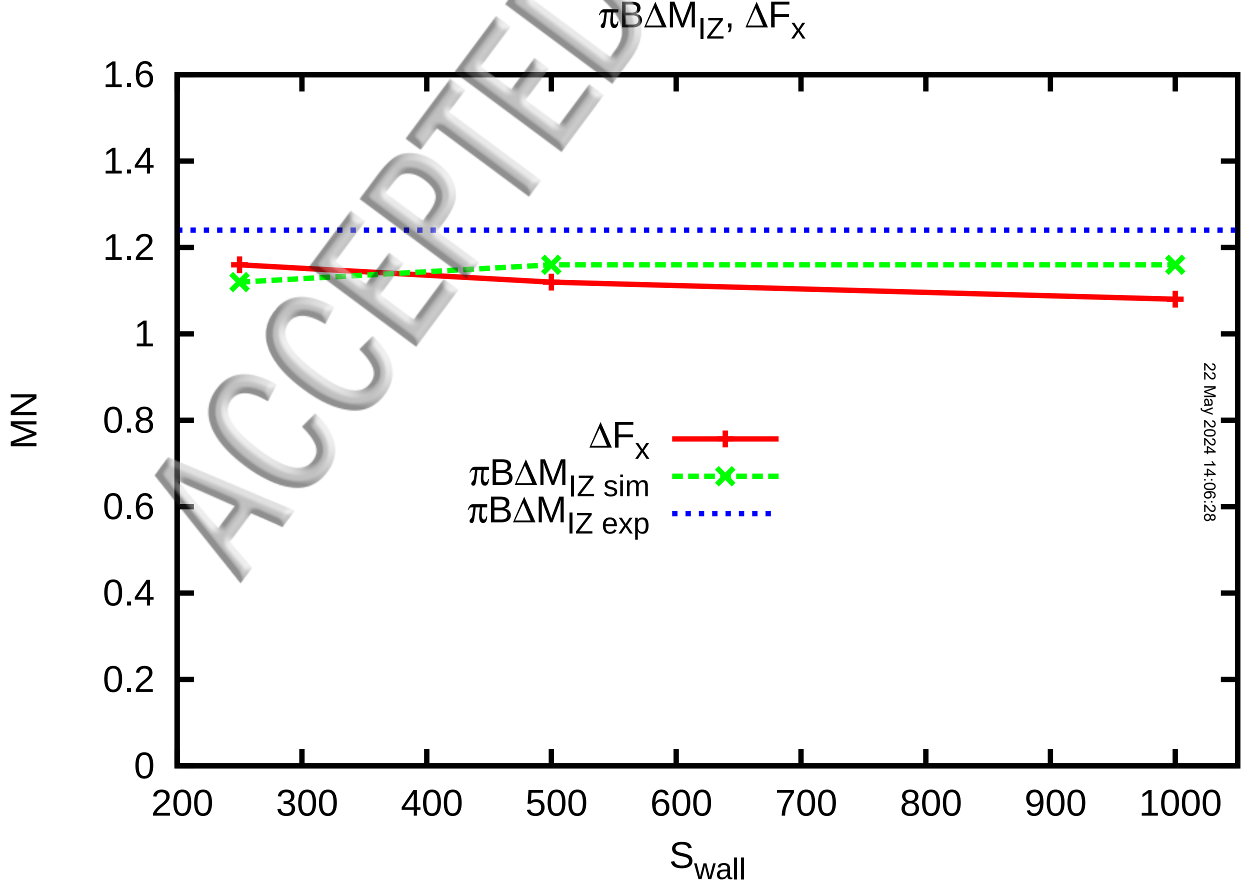
πBΔM_IZ, ΔF_x
1.6
1.4
1.2
1
0.8
0.6
0.4
0.2
0
MN
200
300
400
500
600
700
800
900
1000
S_wall
ΔF_x
πBΔM_IZ sim
πBΔM_IZ exp
22 May 2024 14:06:28

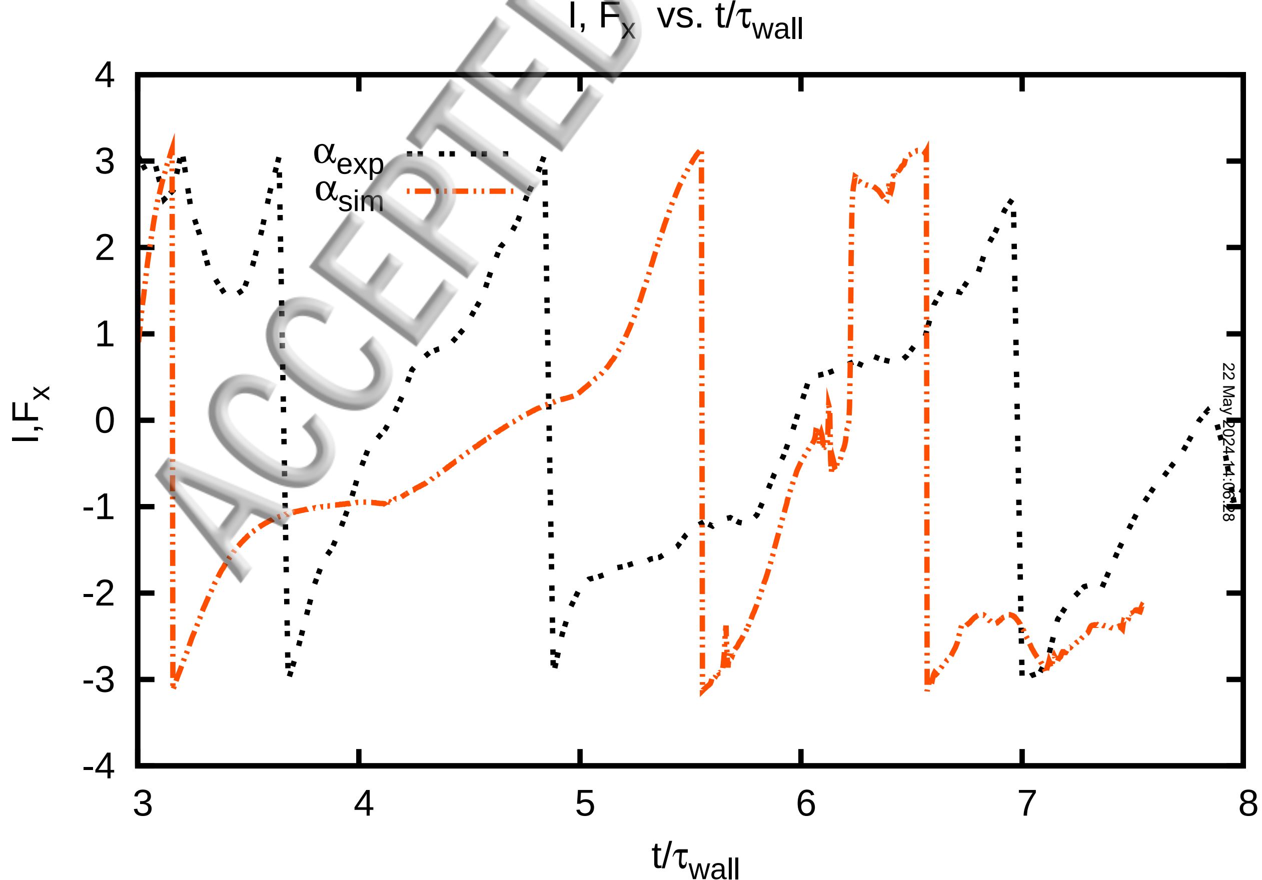

I, F_x vs. t/τ_{wall}
α_{exp}
α_{sim}
I,F_x
t/τ_{wall}
4
3
2
1
0
-1
-2
-3
-4
3
4
5
6
7
8

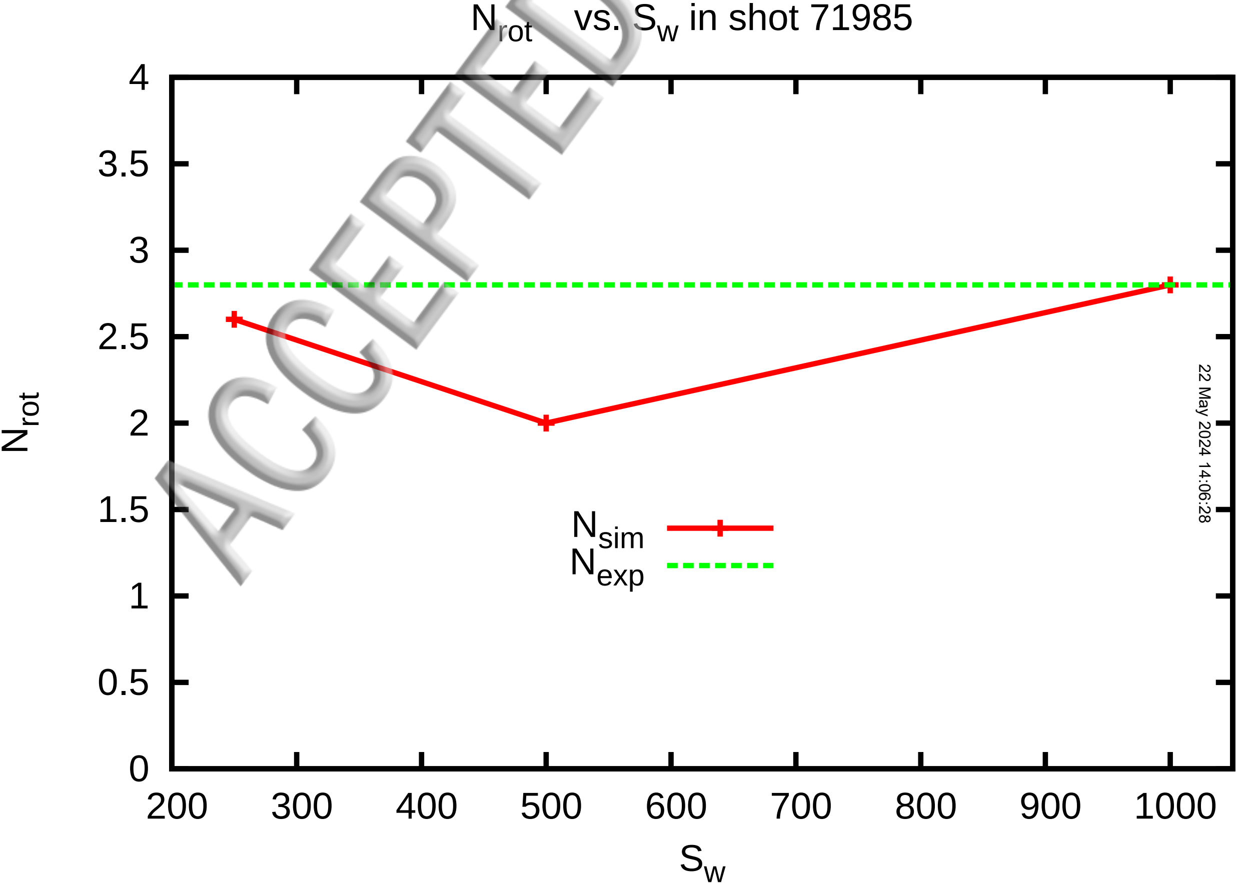

N_{rot} vs. S_w in shot 71985
4
3.5
3
2.5
2
1.5
1
0.5
0
200
300
400
500
600
700
800
900
1000
S_w
N_{rot}
N_{sim}
N_{exp}
22 May 2024 14:06:28

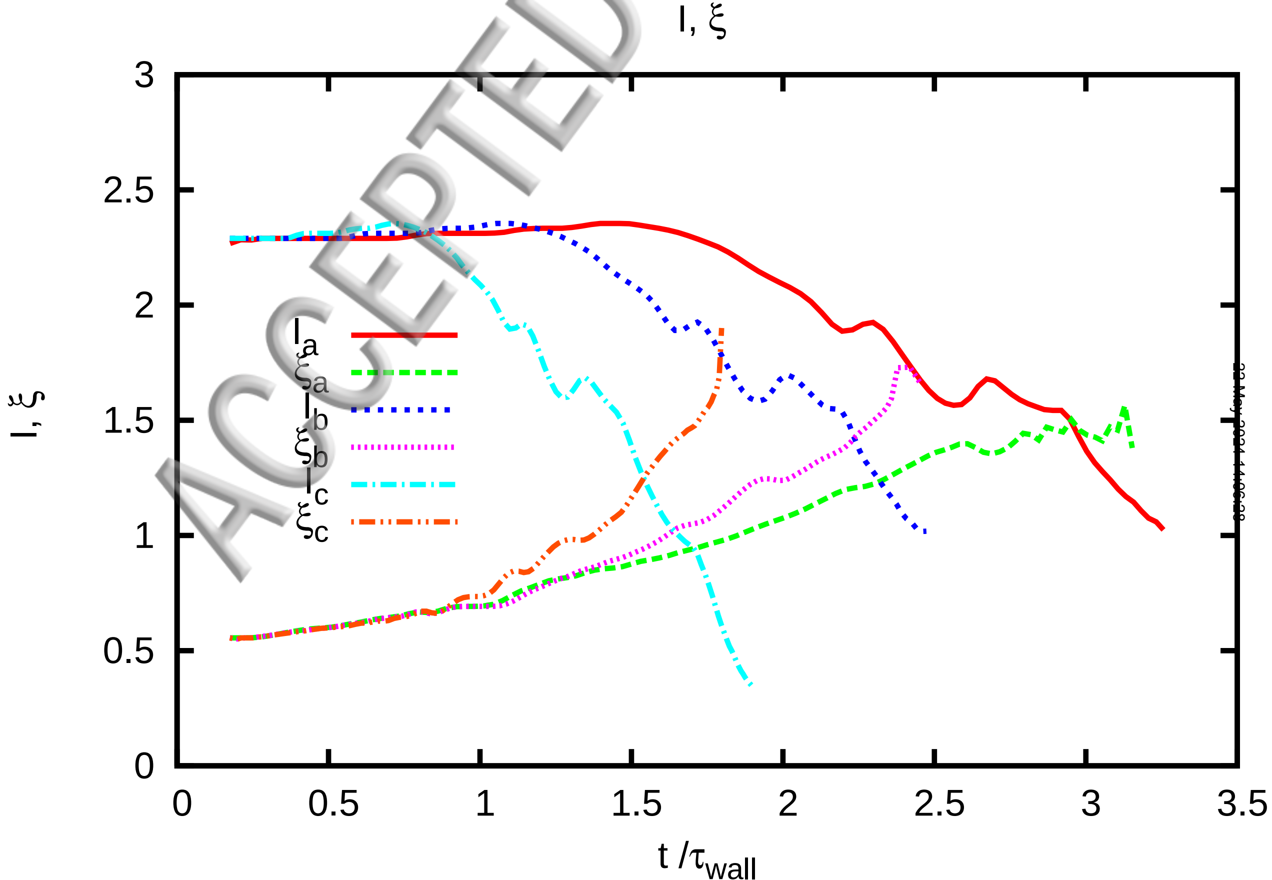

l, ξ
3
2.5
2
1.5
1
0.5
0
0
0.5
1
1.5
2
2.5
3
3.5
l, ξ
t /τ_wall
l_a
ξ_a
l_b
ξ_b
l_c
ξ_c
22 May 2024 14:06:28

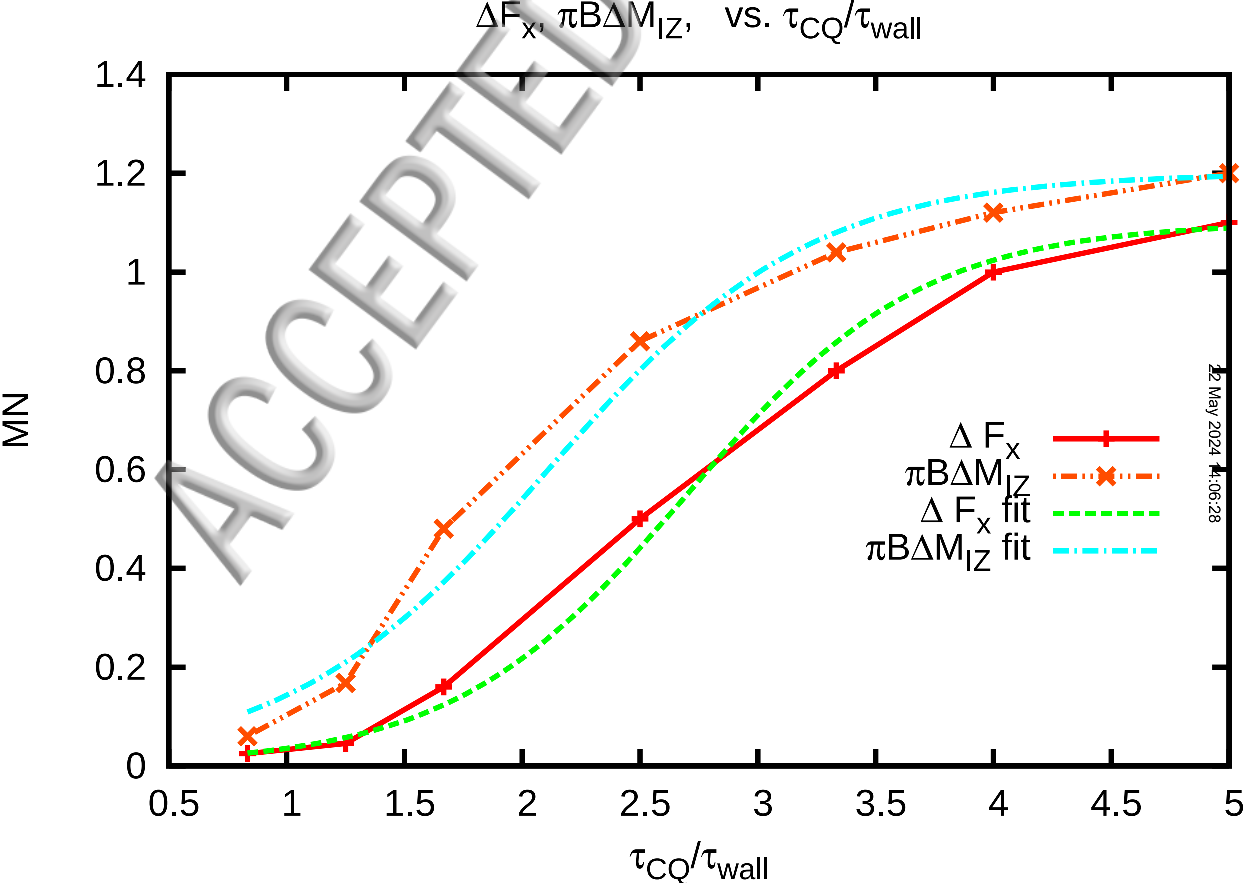

ΔFx, πBΔMIZ, vs. τCQ/τwall
MN
τCQ/τwall
1.4
1.2
1
0.8
0.6
0.4
0.2
0
0.5
1
1.5
2
2.5
3
3.5
4
4.5
5
Δ Fx
πBΔMIZ
Δ Fx fit
πBΔMIZ fit

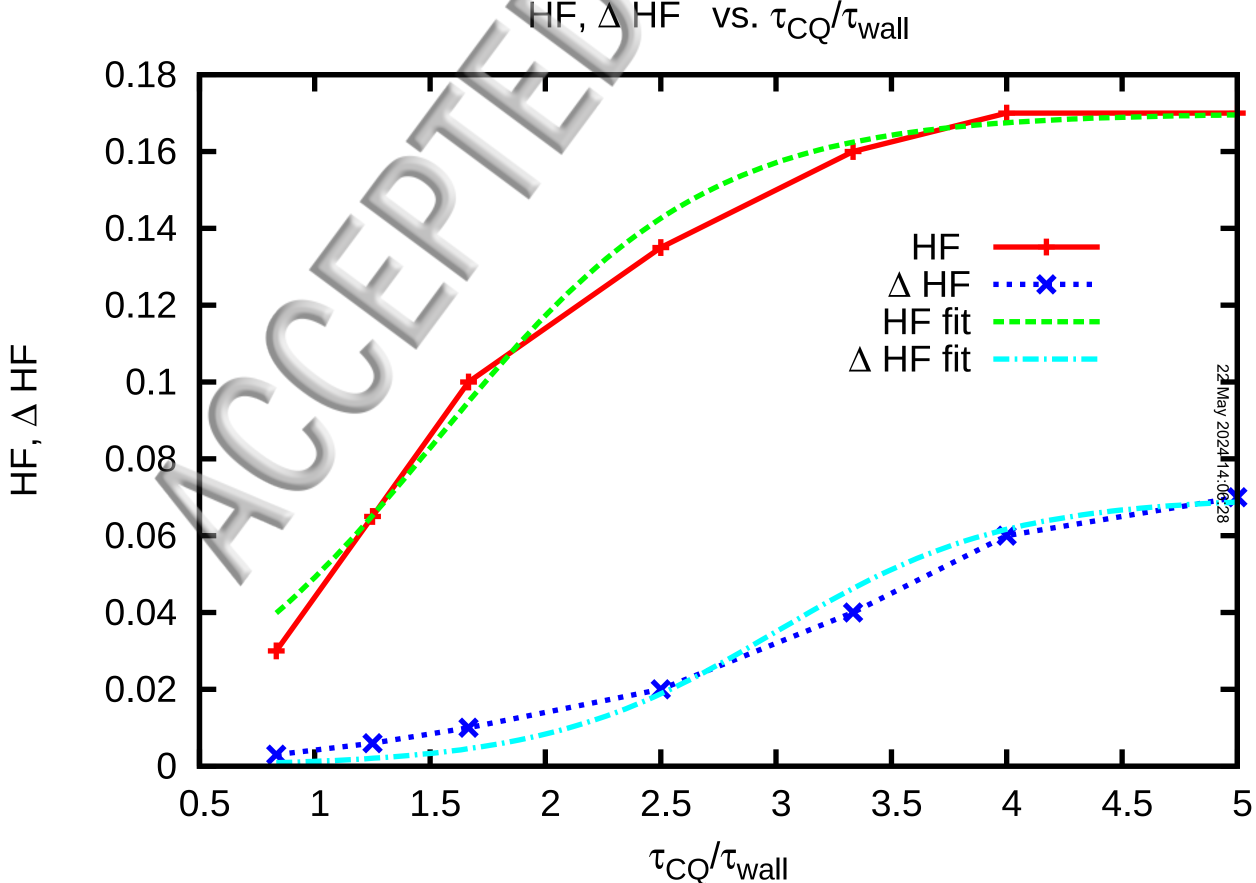
HF, Δ HF vs. τCQ/τwall
HF, Δ HF
τCQ/τwall
0
0.02
0.04
0.06
0.08
0.1
0.12
0.14
0.16
0.18
0.5
1
1.5
2
2.5
3
3.5
4
4.5
5
HF
Δ HF
HF fit
Δ HF fit
ACCEPTED
22 May 2024 14:06:28